

Response to Reviewer 1:

The manuscript "Recent Precipitation Decrease Across the Western Greenland Ice Sheet Percolation Zone" by Lewis et al. presents large scale GPR transects and accumulation derivations thereof for more than 4400km of the Western GrIS. Such data are combined with firn cores to enable layer dating and accumulation calculations from density measurements. Vertical in-situ data allow accumulation derivations for the last 2 to 6 decades enabling trend assessments. In-situ trends are compared with RCM outputs to analyze for changes in accumulation and precipitation in relation with global temperature changes. The authors describe significant decreases in accumulation rates within the last 2 decades, which they attribute to shifting storm tracks reducing precipitation mainly for the summer months and increasing surface melt. I consider the presented work as novel and certainly significant for the scientific community especially because of the extensive data collection presented in this work. However, some redundancies, imprecise descriptions and the confusing structure of the manuscript prevent publication in the current state. I recommend to focus more on conciseness and maybe reconsider the total volume of the presented data. How about splitting into 2 manuscripts: one presenting the in-situ data including validation/ comparison with RCM results and the subsequent dealing with implications and atmospheric circulation simulations. Right now, the reader gets a bit lost in all the error/ uncertainty analyses combined with validation proofs for numerous statistics.

Thank you for your thorough and helpful review. We appreciate that the manuscript covers a great deal of ground between the extensive data collection and climate-based analysis. However, we have decided not to split the manuscript in order to keep the data collection and analysis together. We feel that the background and data collection are necessary to motivate the reader to think about recent GrIS SMB changes. We use the field measurements to validate RCMs, which we then use to examine widespread SMB changes across the whole GrIS. We do not think two manuscripts would be able to portray these important results as accurately as one longer manuscript.

We have shortened the manuscript and reduced the length of several sections, particularly the introduction, to reduce the total volume of information. We believe that the manuscript is more concise and will nicely fill a gap in the literature of recent GrIS SMB measurements.

Major points of criticism are: The structure of the manuscript is very confusing. The methods section comprises large fractions of discussion and data interpretation. Please revise the structure and attempt to shorten the manuscript whenever possible.

We agree that some of the text originally in the methods is too verbose and is not appropriate for this section. Specifically, we removed material about the average relative permittivity, clarified how meltwater percolation effects isotope signals, added a sentence about comparing thermistor measurements with MODIS satellite derived temperatures, and removed a sentence within the leave-one-out cross validation paragraph. We feel that the radargram and density plots, while technically results from this study, belong in the methods section because they help the reader better understand the accumulation calculations and TWT-depth conversions.

The introduction comprises almost 3 pages. It is clear to me that you want to introduce all relevant literature and topics, which are presented. However, if splitting into 2 manuscripts (see

above), you could certainly focus more on less different topics. Parts, which could be shortened are L54ff and L89ff.

We have shortened the introduction from three pages to two pages and removed unnecessary background material. We have shortened much of the material discussed in L54-L89 because Greenland summertime melting has previously been thoroughly discussed in the literature and does not need to be explained here in great detail. We appreciate this feedback and feel it has made the manuscript more concise.

At least to me, it remains unclear how specific values are determined. For instance, epoch and annual accumulation values are hard to distinguish. It would be better to clearly distinguish in between these two.

Annual accumulation is determined from the firn core chemistry data and is only shown in the background of Figure 5. We do not use discuss individual annual accumulation rates in this manuscript.

Epoch accumulation (average accumulation over multiple years) is calculated from adjacent IRHs (equation 3) in the geophysical data across the entire GreenTrACS traverse. We use these values to determine changes in accumulation in sections 3.4 and 3.5. We changed L330 to “We assume uncertainty in dating the firn cores from annual variations in chemistry...” to clarify this point.

Did you actually pick each individual layer in the radar data or just for specific locations where layer resolution is clear or just the 5 year layers as indicated in Fig. 5? This remains unclear, same for the accumulation calculations.

As can be seen in Figure 3, we trace these individual layers across the dataset wherever the penetration depth (and equipment malfunctions) allows us to do so. Accumulation is calculated everywhere along the GreenTrACS traverse.

We have added to L269-271: “Each horizon is traced throughout the traverse, except in areas where the attenuated signal makes it too difficult to interpret.”

You state that 1m fractions as well as 3cm parts of the cores are analyzed (L233ff) in the field and lab. Were those core fragments further cut for more highly resolved density measurements?

Core fragments were measured and weighed in the field as well as in the Dartmouth College Ice Core Laboratory freezer to calculate depth-density profiles. We repeat these measurements in case cores are lost or melted in transit, to double check for measurement errors, and to reacquire measurements in a controlled laboratory setting. We measured pieces along natural core breaks during the drilling process and did not further cut these pieces for higher resolved density measurements. For more information see Graeter et al. (2018).

In addition, average melt rates in Fig. 11 and discussed in Section 3.5 are not adequately explained. I don't see how such values are generated (derived from RCMs, calculated in accordance to observed ice lenses as in L581?).

Melt rates were measured from collected firn cores and published in Graeter et al. (2018). We measured ice layer thickness for each core using a light table in the Dartmouth College Ice Core Laboratory freezer. We then total the ice layer thickness per year using the chemistry derived depth-age scales.

We have added text to L213-214: “We measured melt layer thickness in the laboratory following Graeter et al. (2018).”

RMS values describing deviations from RCMs lack an explanation for the uncertainty range. **We have added the following text to L466-468 “Averaged over all 4436 km of the traverse, the RMS difference ($\pm 1\sigma$) between each model and GreenTrACS accumulation over corresponding data periods...”**

In summary, I must admit, I got lost with all the uncertainty values being presented. What are sigma_epoch errors, how are these values related to sigma_accumulation-rate? I recommend to work carefully on the respective sections and maybe include a sketch of the applied workflow to derive accumulation data from radar IRHs.

σ_{epoch} is the uncertainty in accumulation rate for any single epoch. This combines all the individual uncertainties discussed in section 2.6 into one general uncertainty that we can use to compare our accumulation rate for a specific epoch with RCM accumulation rates. $\sigma_{n-epochs}$ is the uncertainty in accumulation rate for multiple epochs. We use this uncertainty when comparing our accumulation rate over multiple epochs with RCM accumulation rates.

We have clarified equations 5 and 6 to simplify these complicated concepts.

L341-350 now reads “We find the total accumulation rate uncertainty for each epoch to be 0.0709 m w.e. a⁻¹ from equation 5.

$$\sigma_{epoch} = \sqrt{b^2 \left(\left(\frac{\delta h}{\Delta h} \right)^2 + \left(\frac{\delta t}{\Delta t} \right)^2 + \left(\frac{\delta \rho}{\rho} \right)^2 \right)} \quad (1)$$

... To calculate uncertainty for accumulation averaged over multiple epochs ($\sigma_{n-epochs}$) we divide our uncertainty σ_{epoch} by the square root of the number of traced layers (n) at that location.

$$\sigma_{n-epochs} = \frac{\sigma_{epoch}}{\sqrt{n}} \quad (2).”$$

Just for clarification: The accumulation rate uncertainty is 71kg/m2/a, I interpret this value as the max accuracy you can achieve from GPR transects The RMS deviation to IceBridge accumulation rates is 39kg/m2/a, which is within the error margins. For annual accumulation rates in Fig. 5, I would expect to have error margins as stated above being included. How reliable is a 5-year standard deviation in accumulation rates?

Thank you for the clarification question. The GPR accumulation rate uncertainty for any single epoch is 0.0709 m w.e. a⁻¹ and the average RMS difference from IceBridge accumulation rate is 0.0387 m w.e. a⁻¹, so they are statistically indistinguishable from each another.

The error bars in Figure 5 represent those uncertainties.

The five-year standard deviation in firn core accumulation rates accurately captures the variability of year-to-year fluctuations in accumulation throughout this region.

The RMS deviation to RCMs is 48-82kg/m2/a and again within the error margins of the radar. Annual trends in precip are at 7kg/m2/a2. Consequently, you would need at least a 10 year period to reach the error margins for deriving trends, right?

You are correct in that the average RMS difference from RCM accumulation is 0.0475 to 0.0822 w.e. a⁻¹, although these differences are much larger in certain regions of the traverse (see Figure 9).

Our GPR accumulation trends are 0.009 ± 0.005 m w.e a⁻² from 1996 to 2017, while RCM accumulation trends are 0.0016 to 0.003 m w.e a⁻² larger than that. While these trends are an order of magnitude smaller than the RMS difference between GPR and RCM accumulation, we have shown both the validity of our measurements and their agreement with RCM trends. Therefore, we are confident that both our measured trends and RCM trends exist.

How is the vertical resolution limit of the 400MHz antenna calculated? For firm of $\rho_{\text{ice}}=550$ kg/m³ you would receive a v_{mean} of 0.2m/ns resulting in a wavelength of 0.5 m. Resolution limits are sometimes defined as half of the wavelength or $1/4 \cdot \lambda$. How do you come up with 0.35m?

The interface separation resolution is defined by the bandwidth, which controls the pulse duration, and not the center frequency (see Appendix C of Marshall and Koh., 2008, which is applicable to both FMCW and impulse radars). GPR systems usually have a bandwidth on the order of the center frequency. For a velocity of 0.2 m ns⁻¹, we can use the equation for range resolution, $v/(2 \cdot \text{bandwidth}) = 25$ cm. We could not distinguish separate features within less than 0.35 m in our radargrams, so we conservatively choose a resolution limit of 0.35 m.

You discuss several times errors introduced by percolating melt water. Heilig et al. (2018) measured the seasonal mass flux from snow into underlying firn at Raven to be at >50 kg/m² (in your preferred units >0.05 m w.e.) for summer 2016. Can you clearly date back ice lenses or is the mentioned ice lens from 2003/04 a result of several melt seasons? What about summer 2012? Shouldn't there be a thicker ice lens arising from this melting event? How deep did water percolate within this summer season? I would expect at least a paragraph dealing with such uncertainties, apart from the given uncertainty of 0.5a for layer dating, which represents a strange value dealing with IRHs generated from end-of-melt-season surfaces.

We cannot be confident dating the ice lenses to a particular year, as meltwater typically percolates to depths greater than 1 m (Benson, 1962; Cox et al., 2015; Harper et al., 2012). The ice layer located within any given year may have been generated from that year or a following year. However, we can confidently date the surrounding snow, as the oxygen isotope and major ion signals remains relatively unperturbed (see Neff et al., 2012 – Journal of Glaciology; Avak et al., 2018 – Journal of Glaciology).

We have updated the text to “While meltwater percolation smooths the signal of some of these tracers, we can still confidently determine the depth-age curve using nearly-unperturbed oscillations in $\delta^{18}\text{O}$ and dust.”

The ice lens from the 2012 event is likely thicker throughout the traverse than ice lenses from other summers. We can still confidently calculate SMB over 5 year periods from this method by analyzing the amount of mass between adjacent IRHs.

The 0.5 year uncertainty arises from dating the firn core using isotope and major ion chemistry, not from counting IRHs annual layers like Medley et al. (2013) or Koenig et al. (2016).

The layer picking remains a bit unclear. What happened for the 2011 IRH after Core 14? The indicated layer is almost horizontally flat, which certainly does not correspond to the layers underneath or above. Zooming in, I cannot follow the 2011 tracked reflection horizon. I would certainly pick the IRH from 2014? or 2010? layer instead, which are much more prominent. Can you comment on this?

The resolution of this image is too low to clearly see the undulating IRHs along the 2011 layer. We have double checked the layer picks in Figure 2 and observed a small error in the 2011 layer. We have fixed that IRH and recalculated accumulation across that region, noting that none of the accumulation measurements change by more than 0.01 m w.e. a⁻¹. After reexamining the rest of our layer picks, we are confident that they are correct. Note that we will publish both our GPR data and layer picks with this manuscript so that others can verify our interpretation of the data.

This image serves as a subset of the traced IRHs from the entire 2017 traverse to highlight the high spatial resolution of our dataset. We purposefully traced these IRHs throughout the dataset rather than tracing specific prominent horizons for short distances.

Values in Section 2.2 are not correct. Here, you mixed up digits a bit. A RELATIVE DIELECTRIC (please consistently use this phrase) permittivity of 1.26 would correspond to a bulk density of $\rho_s=145\text{kg/m}^3$, which is certainly not the case for firn. Please correct accordingly and also correct the derived depth ranges.

Thank you for pointing out this error. We have corrected the usage to “relative dielectric permittivity” throughout the manuscript.

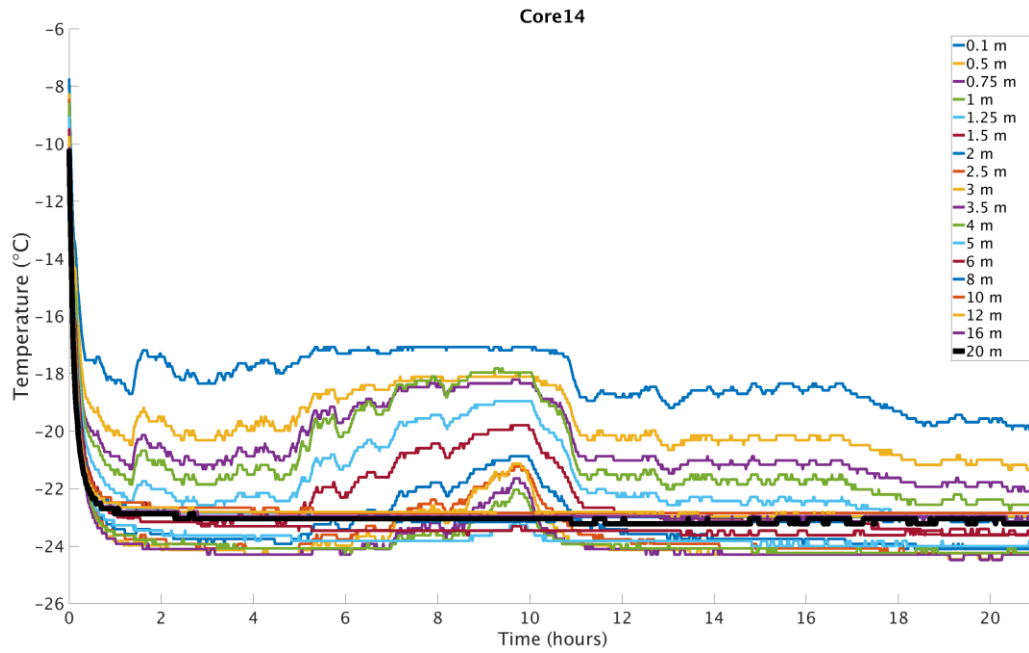
We have removed this sentence entirely as it is confusing to the reader. The derived depth ranges were not calculated using a constant relative dielectric permittivity, and are not affected by this error.

There are several parts, where I would like to see quantifications (e.g., L24, L132, L169, L475). **We have added quantifications to these locations to indicate the recent decrease in accumulation. The text now reads “...show decreasing accumulation and precipitation of $2.4 \pm 1.5 \text{ \% a}^{-1}$ ” and is easier to understand.**

Thermistors in boreholes need to settle before they can provide reliable numbers. I can see that this is impossible for the field approach you chose but can you provide comparisons of thermistor with MODIS annual temps? You should at least mention difficulties of an open borehole for temp data.

Correct that borehole thermometry is usually conducted over periods longer than 24-48 hours. However, the thermistor at 20 m depth (thick black line on figure below) is able to asymptotically equilibrate within 24 hours to within $\pm 0.1 \text{ }^\circ\text{C}$ and provides a temperature that we are confident can be used to drive a Herron-Langway density profile. Please see an example of the data from Core 14 below.

We added the following text to L225: “These measurements agree with MODIS satellite derived mean annual temperature (Hall et al., 2012) to within $\pm 1 \text{ }^\circ\text{C}$ for each firn core location.”



Please revise the manuscript carefully for punctuation marks. I found numerous missing commas.

The manuscript has been revised for missing commas.

Response to Reviewer 2:

GENERAL OVERVIEW: Lewis et al. work titled “Recent Precipitation Decrease Across the Western Greenland Ice Sheet Percolation Zone” reconstructs annual accumulation rates by using a well-known method of combining snow/firn density profiles from ice cores with the depth at which radar isochrones are found; in the dry-snow zone, radar isochrones are related to the depth-hoar formed at the end of summer, effectively marking annual accumulation layers. Here, they use the methodology in the percolation zone, and compare results with those of regional climate models to conclude that precipitation rates in the percolation zone of western Greenland show a decreasing trend. The data presented is of interest, and the radar data obtained over the percolation zone is certainly of importance. The paper is well written and clear, and I have few corrections regarding that. The methodology is well described, but I do however have some comments regarding the validity of the it given the interpretation of results. The paper could also do a better job summarizing recent studies in the area; this needs to be addressed to avoid any impression that authors are cherry-picking results to reinforce their conclusions. Only Overly et al. findings are quoted using a similar method, but there are several studies showing that accumulation rates are increasing in this area (e.g. Koenig et al.).

Thank you for your review and comments, we believe they have made the manuscript stronger and more succinct. Our introduction covers all recent *in situ* radar studies in this region and we are the first to collect data throughout many regions in the traverse. We highlight several studies that use similar methods (e.g. Hawley et al., 2014) and studies using other methods that found different results (e.g. Wong et al., 2015; Overly et al., 2016).

Our results are statistically indistinguishable from those of Koenig et al. (2016; not shown) over 2009-2012. Our accumulation trends from 1996-2016 cover a longer duration than the data from that study and their accumulation trends are almost all statistically insignificant. Koenig et al. (2016) discusses increased accumulation near Camp Century only within the MAR RCM, which “differ in magnitude from the radar-derived measurements in 2010 or 2011.”

The following text has been added to section 3.2 “Similarly, our 2011-2016 accumulation is statistically indistinguishable from average 2009 – 2012 IceBridge snow radar measurements analyzed by Koenig et al. (2016), with an RMS difference of 0.0489 ± 0.0961 m w.e. a⁻¹ along a total of 69.7 km of overlap (not shown). Koenig et al. (2016) use a different radar system on an airborne platform and are able to calculate annual accumulation at elevations below 2000 m a.s.l., however the GreenTrACS accumulation record covers a much longer temporal duration than the data from that study.”

There is too much emphasis on the comparison with IceBridge radars, but clear differences between the VHF pulse radars and microwave phase-sensitive radars must be made because they operate differently. **The following text has been added to the introduction “Note that our *in situ* GPR operates using a UHF pulsed radar, while other systems such as frequency modulated continuous wave (FMCW) radars use phase-sensitive radar architecture that include both amplitude and phase information.” While the pulse and phase-sensitive radars operate differently, the radargrams generated by pulse radars within the VHF-UHF spectrum allow us to trace isochronous IRHs and calculate accumulation, in a similar way to the airborne FMCW approach. In dry snow/firn, the relative dielectric permittivity is not sensitive to frequency in the range between UHF and microwave, and therefore the radar velocity is not influenced by the different frequencies of these systems.**

Although the uncertainties in the shallow firn core data are well explained, there is not sufficient details on the radar uncertainties, which are definitely large enough. This can even be seen at the sites where the shallow firn cores were taken (e.g. Figure 5).

A detailed explanation of the radar uncertainty can be found in Section 2.6.

Figure 5 shows that radar and firn core accumulation measurements are statistically indistinguishable at four example core sites, which is also the case at all sixteen core locations. We

believe that these uncertainties are small enough to allow for analysis of accumulation trends in our dataset.

In my opinion, the emphasis should not be so much decreasing accumulation, which the authors hypothesize is caused in part by blocking of storms in the summer; the models only show a very slight decrease when looking at decadal trends, and the differences with the radar-estimated rates are larger than that, even over the core sites (Figure 5).

Although the decrease in accumulation is small, we show throughout the manuscript that it is not negligible. Furthermore, the general narrative in the literature is that accumulation is increasing, and will continue to increase, with higher human-forced temperatures due to higher saturation vapor pressures. We show that this is not the case over the past two decades in our study region, and we point to the importance of summer blocking as a driver of the accumulation decline, which has not been discussed extensively in the literature. We emphasize the accumulation decline because none of the CMIP5 GCMs can accurately capture recent Greenland blocking activity (Hanna et al., 2018), and our results highlight that mass loss is currently occurring from both sides of the SMB equation (declining mass input, and accelerating mass output from melting and runoff). We therefore respectfully disagree that this should not be emphasized in the paper; we believe that it is the most important contribution that this paper makes to our understanding of Greenland SMB.

Section 2.2. How do you differentiate between annual accumulation layers (depth hoar formed in September/October) from percolation layers formed during the summer? As stated, unlike phase-sensitive radars, GSSI pulse radars can penetrate ice layers if they are thin enough, but without power analysis they look the same as depth hoar.

We do not differentiate between annual accumulation and percolation layers. Rather, we calculate accumulation between adjacent IRHs using the age and mass between these isochrones, determined from the depth-age scales and densities interpolated from the firn cores. The SMB is indifferent to where the mass originated, all we're trying to do is calculate that mass balance.

Ln 157 A radar isochrone is by definition continuous IRHs, so this is redundant. What you really mean is that the isochrones observed have been related to annual accumulation layers.

We have updated the text to reflect this distinction. The text now reads “The 400 MHz short-pulse radar has a range resolution (ability to resolve distinct features) of 0.35 ± 0.1 m in firn, which is fine enough to resolve Internal Reflecting Horizons (IRHs) that have been related to annual accumulation layers (Medley et al., 2013; Rodriguez-Morales et al., 2014; Spikes et al., 2004; Hawley et al., 2014).”

Ln 233 Why is the diameter needed? isn't the diameter of the cores approximately the same? If this is due to irregularities in the shape core, then it has to be explained that the core is assumed to have a cylinder-like shape with measured diameter.

The diameter of the core fluctuates slightly (<1 mm), so to accurately calculate the volume and density of each core section we measure the diameter of the core at the beginning, middle, and end of that section using calipers. Since the radius is squared in the cylinder's volume calculation, it is imperative to know the radius as accurately as possible for density calculations. For more information see Graeter et al. (2018).

Ln 253-254. This phrase is not clear; please explain better.

The text has been modified to “Final calculated accumulation rates are insensitive to the input accumulation parameter we use to calculate our Herron-Langway models (Lewis et al., 2017).”

Ln 256-260. It is really hard to believe this statement without more in-situ data. As a matter of fact, there are studies that show that 21st Century percolation facies not only consist of pipes and lenses, but widespread layers that do amount to a fraction of the total accumulation (Perry et al., 2007; Helm et al., 2006; de la Pena et al., 2015; Machguth et al., 2016). At the very least, an assessment of the uncertainties related to this should be given.

These studies are all from lower elevations on the ice sheet, where certainly the reviewer is correct that ice lenses can be widespread and account for a significant fraction of the year's total accumulation. At the higher elevation of our firn cores, however, we did not observe widespread ice lenses across the snow pits used to extract cores, snow pits used for stratigraphic analysis, or snow pits used for camp. Cores 1 – 7 had an average of 1 – 5 cm total ice layer thickness per year, while cores 9 – 16 had less than 2 cm of melt per year, most of which occurred during the past decade.

Section 2.4. Is this different as what is shown in Figure 2? Section 2.2 states a constant dielectric to estimate depth. Please clarify.

We have removed the sentence in Section 2.2 that made it appear we were using a constant relative dielectric permittivity to estimate depth. In actuality, we calculate permittivity from the density (equation 2) in order to calculate the velocity (equation 1) so that we can determine depth from the TWT.

Section 2.5. It is stated that sometimes a “layer appears to bifurcate...” How does the authors know that the layer being traced is an actual annual layer (e.g. a depth hoar) and not a percolation feature?

We do not distinguish between annual layers and percolation features, rather, we trace IRHs from one firn core to another in order to calculate SMB between the two cores. It doesn't matter what contrast in relative dielectric permittivity is causing the IRH, all that matters is that these horizons are isochronous and we know the date of each layer within ± 0.5 years. If the accumulation rate changes substantially and layers bifurcate multiple times, it would be possible that the traced IRH represents a different part of the year from the original traced layer. Since our epochs represent five years, at most, this could change the length of the epoch by $\sim 10\%$, but we do not have any IRHs between adjacent firn cores that exhibit this behavior.

Ln 313-318. If the range resolution of the radar as stated in Section 2.2 is 0.35 m, then how it is possible that two radar samples are 0.12 m? This is inconsistent. My guess is that the uncertainty in accumulation estimates just from this would be at least the resolution times density, which is much higher than what is stated here.

The range resolution (ability to distinguish distinct features) is 0.35 m, and is controlled by the radar bandwidth, but the radar sample spacing, which is controlled by the sample frequency of the analog to digital converter, is 0.12 m. We cannot definitively distinguish which range bin the IRH lies within, hence our uncertainty of 0.35 m. The resulting uncertainty in accumulation is $0.0709 \text{ m w.e. a}^{-1}$, accounting for uncertainties in radar precision, tracing IRHs, errors in dating the firn cores, and errors in our density estimates.

Ln 325-326. But it was stated in Section 2.3. that variable percolation facies do not affect estimates. I know is further discussed in Section 3.5, but my opinion is that more emphasis should be made in the variable structure of firn over the percolation zone.

In this paragraph we are saying that the difference between calculating accumulation using measured density profiles and calculating accumulation using estimated/interpolated density profiles has larger errors for the southern cores because meltwater percolation and ice lenses complicate the density profile. We have added the following text to L316-317 “Throughout this study, we use our measured density profiles to calculate accumulation at core locations, rather than rely on Herron-Langway density models that would result in larger uncertainties.”

Numerous studies have documented the heterogeneity of firn throughout the percolation zone and the complications of calculating SMB due to ice pipes and lenses. Here we attempt to accurately calculate accumulation using firn cores and *in situ* GPR throughout this complicated region. The text has been updated to reflect these complications.

Ln 673-674. Please provide references.

We have added references for these climate models. This sentence now reads “Overall, the Polar MM5 (Burgess et al., 2010), MAR (Fettweis et al., 2016), Box13 (Box et al., 2013), and RACMO2 (Noël et al., 2018) Regional Climate Models accurately capture large spatial patterns in accumulation over the GrIS, but show statistically significant differences from GPR accumulation on a regional basis.”

Ln 677-678. I do not believe this statement is correct. Uncertainties in radar-derived rates are in my opinion much larger.

Please see section 2.6, and specifically equation 5, for formal error propagation and uncertainty calculations. We believe that we have done everything to accurately constrain the accuracy of this radar system and have been conservative in our uncertainty analysis. For comparison, Hawley et al. (2014) calculate an accumulation uncertainty of ~ 0.015 m w.e. a^{-1} using a similar geophysical system, Overly et al. (2016) calculate an accumulation uncertainty of 0.01 m w.e. a^{-1} using the ASIRAS airborne radar, and Medley et al. (2013) calculate an accumulation uncertainty of 0.055 m w.e. a^{-1} using the IceBridge snow radar. Our total accumulation rate uncertainty for each epoch of 0.07 m w.e. a^{-1} is the same order of magnitude, but larger, than those reported uncertainties.

Figure 1. Please include elevation contour lines, it would be helpful for the reader even if most of the traverse is along an elevation of 2100 masl.

We have added the 2000 m and 3000 m contour lines to Figure 1. We believe these give an idea of the elevation of our traverse without crowding the figure too much.

Figure 5. Please add error bars to the GPR-estimated accumulation.

Error bars in the GPR accumulation are indicated in red. We do not show error bars for the annual core accumulation to simplify the figure, however the error bars for the 5 year averaged core accumulation is indicated in black (GreenTrACS cores) and blue (PARCA cores).

Figure 5 and 12. Please use a larger font size.

We have increased the font size for both figures. These figures are now easier to understand.

Recent Precipitation Decrease Across the Western Greenland Ice Sheet Percolation Zone

Lewis, Gabriel¹; Osterberg, Erich¹; Hawley, Robert¹; Marshall, Hans Peter²; Meehan, Tate²; Graeter, Karina³; McCarthy, Forrest⁴; Overly, Thomas^{5,6}; Thundercloud, Zayta¹; Ferris, David¹

¹Department of Earth Sciences, Dartmouth College, Hanover, NH, USA

²Geosciences Department, Boise State University, Boise, ID, USA

³Office of Sustainability, University of Maine, Orono, ME, USA

⁴College of Fisheries and Ocean Sciences, University of Alaska Fairbanks, Fairbanks, AK, USA

⁵NASA Cryospheric Sciences Laboratory, NASA Goddard Space Flight Center, Greenbelt, MD, USA

⁶Earth System Science Interdisciplinary Center (ESSIC), University of Maryland, College Park, MD, USA

Correspondence to: Gabriel Lewis (Gabriel.M.Lewis.GR@dartmouth.edu)

Abstract

The mass balance of the Greenland Ice Sheet (GrIS) in a warming climate is of critical interest ~~to scientists and the general public~~ in the context of future sea-level rise. Increased melting in the GrIS percolation zone due to atmospheric warming over the past several decades has led to increased mass loss at lower elevations. Previous studies have hypothesized that this warming is accompanied by a precipitation increase, as would be expected from the Clausius-Clapeyron relationship, ~~negating compensating for~~ some of the melt-induced mass loss throughout the Western GrIS. This study tests that hypothesis by calculating snow accumulation rates and trends across the Western GrIS percolation zone, providing new critical accumulation estimates in regions with sparse ~~and/or dated in situ~~ data ~~for calibration of future regional climate models~~ or data that does not span the recent accelerating surface melt. We present accumulation records from sixteen 22 – 32 m long firn cores and 4436 km of ground penetrating-radar, covering the past 20 – 60 years of accumulation, collected across the Western GrIS percolation zone as part of the Greenland Traverse for Accumulation and Climate Studies (GreenTrACS) project. Trends from both radar and firn cores, as well as commonly used regional climate models, show decreasing accumulation and precipitation of $2.4 \pm 1.5 \% \text{ a}^{-1}$ over the 1996 – 2016 period, which we attribute to shifting storm-tracks related to stronger atmospheric summer blocking over Greenland. Changes in atmospheric circulation over the past 20 years, specifically anomalously high summertime blocking, have reduced GrIS surface mass balance through both an increase in surface melting and a decrease in accumulation.

1. Introduction

Greenland Ice Sheet (GrIS) mass loss has accelerated over the past few decades, with modern mass loss rates more than double ~~those at~~ from Antarctica (van den Broeke et al., 2016). The 2010-2018 GrIS mass loss ~~was calculated as~~ $286 \pm 20 \text{ Gt a}^{-1}$ (Mouginot et al., 2019), contributing $0.7 \pm 0.2 \text{ mm a}^{-1}$ of sea level rise. Over

34 the past 20 years, the largest warming rates (Hanna et al., 2012) and fastest mass loss have occurred in
35 Western Greenland ($26 \pm 7 \text{ GT a}^{-2}$ in basins F + G of Sasgen et al., 2012). ~~Here, where regional scale models~~
36 ~~calculate a~~ surface mass balance (SMB) ~~has decreased between ranging from~~ 31.1% (European Centre for
37 Medium Range Weather Forecasting downscaled; ECMWFd) ~~to and~~ 76.5% (Modèle Atmosphérique
38 Régional; MAR) over the 1996 – 2008 period (Vernon et al., 2013) ~~due as a result of to~~ higher surface melt
39 and runoff (van den Broeke et al., 2009, 2016). Modern surface melt rates are at their highest levels of at
40 least the last 450 years across Western Greenland (Graeter et al., 2018) and more broadly throughout
41 Greenland (Trusel et al., 2018). In particular, ice core records from Western Greenland show an abrupt
42 increase in surface melt rates beginning in the middle-late 1990's due to a combination of higher North
43 Atlantic sea surface temperatures, enhanced summertime blocking highs, and anthropogenic warming
44 (Graeter et al., 2018).

45
46 Enhanced GrIS surface melt is driven fundamentally by rising Greenland summer temperature trends as
47 ~~recorded by automated weather stations from the Greenland Climate Network (GC-Net; Steffen and Box,~~
48 ~~2001), coastal weather stations (Box, 2002), borehole thermometry (Polashenski et al., 2014), remote sensing~~
49 ~~(Hall et al., 2008), and ice core stable isotopes (Buchardt et al., 2012). Average annual temperature across~~
50 ~~interior Greenland increased by $0.055 \pm 0.044 \text{ }^\circ\text{C a}^{-1}$ from 2000 – 2012 (Hall et al., 2013), with GrIS summer~~
51 ~~trends upwards of $0.135 \pm 0.047 \text{ }^\circ\text{C a}^{-1}$ (Hall et al., 2013; Reeves Eyre and Zeng, 2017). These warming~~
52 ~~trends extend to the highest elevations of the ice sheet, with and 1982 – 2011 warming at Summit Station of~~
53 ~~$0.09 \pm 0.01 \text{ }^\circ\text{C a}^{-1}$ from 1982 – 2011 (McGrath et al., 2013). Nearly every Greenland dataset shows~~
54 ~~statistically significant positive temperature trends in recent decades, especially during the~~
55 ~~summers~~summertime (Reeves Eyre and Zeng, 2017).

56
57 Basic physics implies that rising temperatures should cause an increase in accumulation over the ice sheet
58 due to the Clausius-Clapeyron relationship – warmer air has a higher saturation vapor pressure, potentially
59 leading to more precipitation (Box et al., 2006; Buchardt et al., 2012). The Coupled Model Intercomparison
60 Project, phase 5 (CMIP5) predicts precipitation increases of 20 – 50% over the GrIS by the end of the 21st
61 century (Bintanja and Selten, 2014), partially offsetting mass loss and sea-level rise from enhanced summer
62 melt and runoff. However, most *in situ* records of Greenland snow accumulation do not span the modern
63 period of rapid warming ~~and accelerating mass loss~~ since the mid-1990s, making it. It is difficult to determine
64 whether accumulation has been increasing with ~~the observed~~ warming temperatures as predicted. For
65 example, the Program for Arctic Regional Climate Assessment (PARCA) campaign collected accumulation
66 data from a network of 49 ice and firn cores ~~46 shallow ice and firn cores in 1997-1998 (<100 m long) and~~
67 ~~three deeper cores (120 – 152 m long) to capture the spatial and temporal accumulation variability over the~~

68 ice sheet (Mosley-Thompson et al., 2001). However, the PARCA firn cores were collected in 1997–
69 1998 (Mosley-Thompson et al., 2001), just at the onset of accelerated surface melting (Graeter et al., 2018).
70 T₁, and the precipitation record from automated weather stations is too brief and localized to analyze
71 significant precipitation trends (Rennermalm et al., 2013). The most recently analyzed deep ice cores (over
72 100 m long) were collected in 2003–2004 (D4, D5, Sandy, Katie; Banta and McConnell, 2007) and there
73 have been no published *in situ* accumulation records from the Western GrIS percolation zone for the past
74 decade. Updated *in situ* snow accumulation data are needed from this region to assess recent changes in
75 accumulation during this period of warming and SMB loss from melt and runoff.

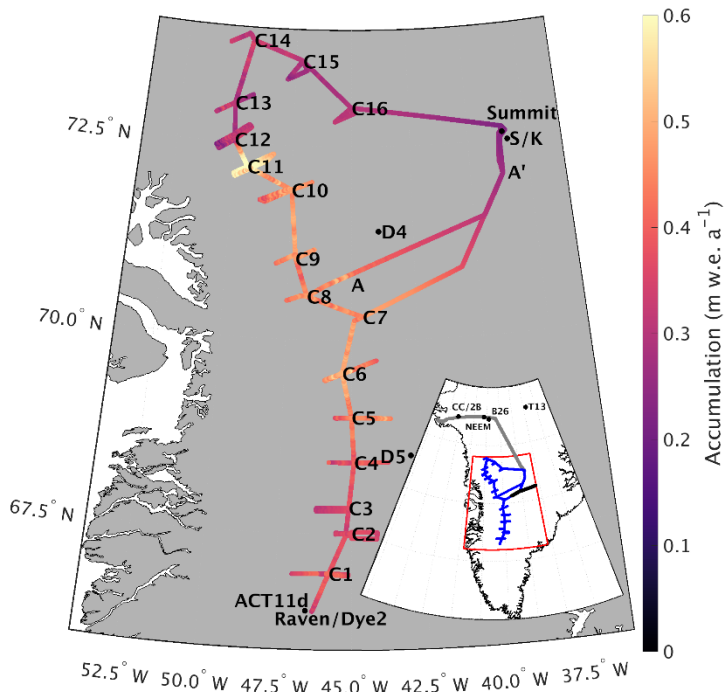
76
77 In addition to measuring snow accumulation with ice cores and automated snow depth sensors, several
78 ~~previous~~ studies have used ground-based and airborne radar to calculate GrIS accumulation rates and trends
79 (e.g. Medley et al., 2013; Spikes et al., 2004; Hawley et al., 2014; Koenig et al., 2016). For example, Hawley
80 et al. (2014) found a 10% increase in northwest coastal Greenland accumulation over the past 52 years using
81 Ground Penetrating Radar (GPR) along the Greenland Inland Traverse (GrIT; see Figure 1 for location),
82 although they did not find any statistically significant trends further inland between the North Greenland
83 Eemian Ice Drilling (NEEM) site and Summit Station. Similarly, Wong et al. (2015) show a coastal increase
84 in precipitation near Thule over 1981–2012, but no statistically significant change in precipitation rate
85 further inland at the Camp Century, B26, or 2Barrel ice core sites. Overly et al. (2016) found a 20%
86 accumulation increase below 3000 m a.s.l. on the historic Expéditions Glaciologiques Internationales au
87 Greenland (EGIG) line from 1994–2004 vs. 1985–1994 using the Airborne SAR/Interferometric Radar
88 Altimeter System (ASIRAS) radar. We build upon these previous studies by collecting GPR data across the
89 lower percolation zone of Western Greenland, where airborne radargrams are often obscured by refrozen
90 melt percolation (Nghiem et al., 2005). Note that our *in situ* GPR used in this study operates using a UHF
91 pulsed radar, while other systems such as frequency modulated continuous wave (FMCW) and ASIRAS
92 radars use phase-sensitive antennas that include both amplitude and phase information. By having our GPR
93 antenna coupled with the snow, we avoid losing energy, and, therefore, penetration depth, from a strong
94 reflection off of the snow-air interface.

95
96 In addition to temperature-precipitation relationships through the Clausius-Clapeyron relationship, previous
97 studies have analyzed the dynamic climate controls on Greenland precipitation. Mernild et al. (2014), Auger
98 et al. (2017), and Lewis et al. (2017) have hypothesized that a positive Atlantic Multidecadal Oscillation
99 (AMO) index correlates with rising accumulation over most of the GrIS interior, since higher sea surface
100 temperatures increase moisture flux over the GrIS and induce greater snowfall. In addition, hHigh pressure
101 (blocking) systems east of Greenland tend to deflect eastward-moving storms over central Greenland and

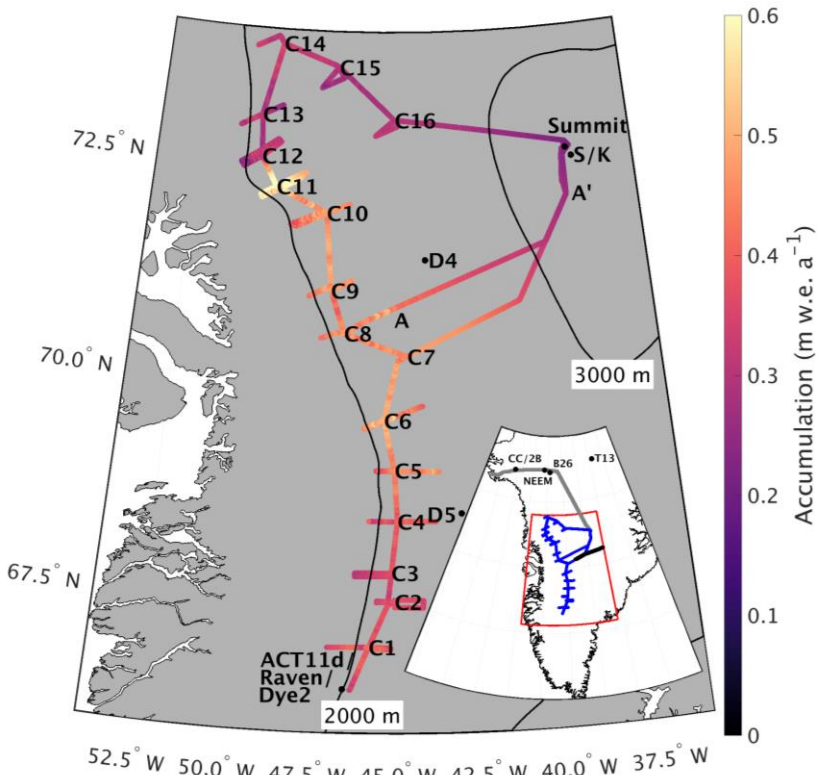
102 increase precipitation, whereas blocking directly over Greenland or in Baffin Bay has the potential to reduce
103 accumulation over the GrIS by displacing the polar jet stream and corresponding storm tracks equatorward
104 prevent storms from crossing the ice sheet (Auger et al., 2017). Over the 1991 – 2015 period there has been
105 particularly strong summertime Greenland blocking (Hanna et al., 2016), but its effects on GrIS accumulation
106 have not been determined with *in situ* data. ~~Through reanalysis data, Auger et al. (2017) showed that~~
107 ~~persistent blocking highs increase precipitation in southwest Greenland and reduce precipitation in the~~
108 ~~southeast.~~

109
110 ~~The Greenland Blocking Index (GBI) quantifies blocking directly over Greenland and is defined as the mean~~
111 ~~500 hPa geopotential height for the 60 – 80°N, 20 – 80°W region~~ (Hanna et al., 2016). ~~Over the 1991 – 2015~~
112 ~~period there has been an especially high Greenland Blocking Index sustained throughout the summers~~ (Hanna
113 ~~et al., 2016). Alternatively, persistent blocking episodes have the potential to reduce snowfall accumulation~~
114 ~~over the GrIS by displacing the polar jet stream and corresponding storm tracks equatorward, although this~~
115 ~~relationship has not yet been documented *in situ*.~~

116
117 Here we develop new accumulation records across the Western GrIS percolation zone using sixteen firn cores
118 and 4436 km of GPR data collected during an over-ice traverse spanning two field seasons. We evaluate the
119 veracity of the accumulation data through comparisons of our firn core time series with previous
120 measurements. We quantify multi-year trends in accumulation across Western Greenland to test the
121 hypothesis that precipitation has recently increased from the Clausius-Clapeyron relationship and higher GrIS
122 temperatures. Further, we assess the ability of RCMs to capture the year-to-year variability and multi-year
123 trends in Western GrIS accumulation. Finally, we evaluate relationships between recent accumulation trends
124 and atmospheric circulation patterns, particularly changes in storm tracks.



126



127

128

129

130

131

Figure 1. Average accumulation across the GreenTrACS traverse for the length of each record showing the location of each firn core, ACT11d, D4, D5, Katie (K), Raven/Dye-2, and Sandy (S) ice cores, and Summit Station. Transect A-A' discussed in Section 3.3. Inset shows locations of Camp Century (CC), 2Barrel (2B), NEEM, B26, and TUNU2013 (T13) ice cores, as well as locations of EGIG (black), GrIT (grey), and GreenTrACS (blue) traverses.

132 **2. Methods**

133 This study uses data from the 2016 – 2017 Greenland Traverse for Accumulation and Climate Studies
134 (GreenTrACS), which measured accumulation and melt across the Western GrIS percolation zone over two
135 summer snowmobile traverses (closely following the 2150 m a.s.l. elevation contour). The May – June 2016
136 season traversed 860 km from Raven/Dye-2 northward to Summit Station, ~~while and~~ the May – June 2017
137 traverse made a 1230 km clockwise loop starting and ending at Summit Station (Error! Reference source
138 not found.Figure 1). This manuscript focuses on accumulation rates derived from 400 MHz GPR data
139 collected along the entire traverse path, as well as sixteen shallow (22 – 32 m ~~long~~deep) firn cores spaced 40
140 – 100 km apart along the backbone of the traverse (Error! Reference source not found.Figure 1). Firn Cores
141 1 – 7 were collected in 2016 and Cores 8 – 16 were collected in 2017. We returned to the Core 7 location at
142 the beginning of the 2017 traverse to recover a weather station and to connect the two season’s GPR data.
143 Additionally, we collected GPR data ~30 – 70 km east and west of each core site, hereafter called “spurs”,
144 to measure changes in accumulation ~~changes~~ along strong elevation gradients (see Error! Reference source
145 not found.Figure 1).

146 **2.1. GPS Positioning**

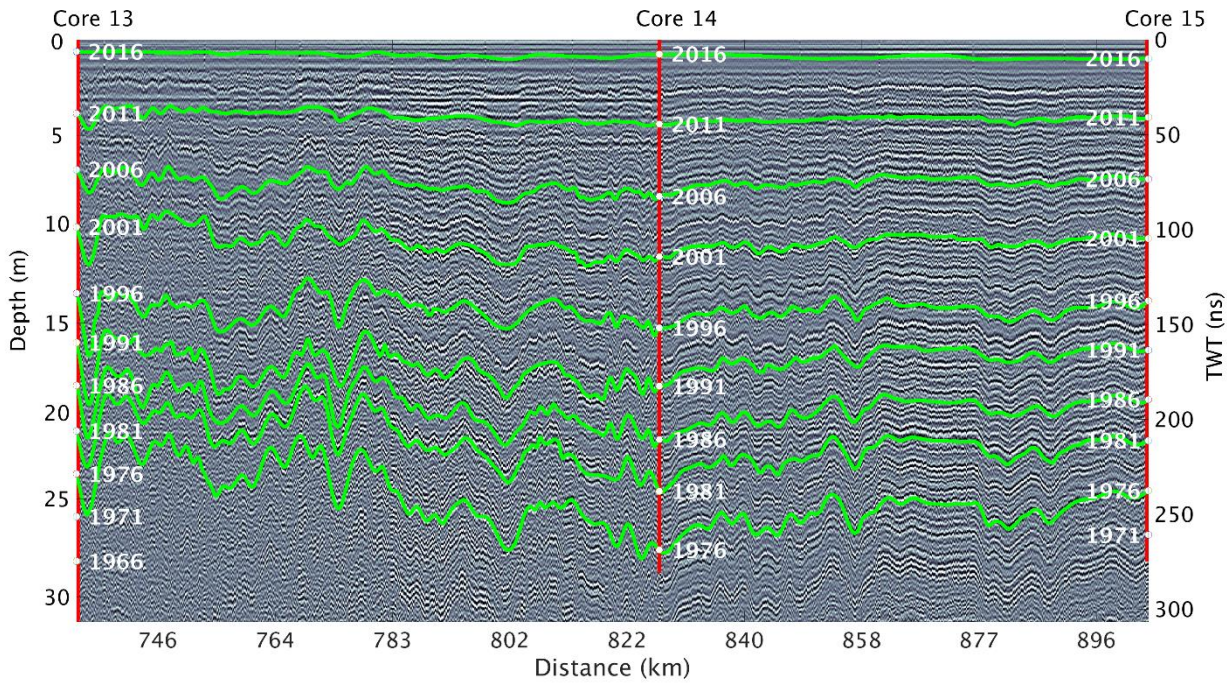
147 During the 2016 traverse we collected GPS data using a Trimble NetR8 reference receiver with a Zephyr
148 Geodetic antenna mounted to a Nansen sled ~5 m in front of the GPR antenna. For each spur and the tail
149 ends of each transect between core sites we performed differential corrections to the GPS data using RTKLIB
150 2.4.1 and a Trimble NetR8 base station near the core site. Between spurs, when not operating a base station,
151 we post-processed GPS data in precise point positioning mode (Zumberge et al., 1997). Estimated root-mean-
152 square horizontal errors were generally between 13 and 18 cm from standard deviations calculated during
153 stationary periods at the end of spurs. To co-register GPR and GPS data, we used time stamps embedded in
154 the two data streams and locations where we stopped to save GPR files, approximately every 15 km. The
155 time drift in the GPR logger is negligible over these durations.

156
157 During the 2017 traverse we used GPS data from a Garmin 19x GPS receiver wired directly to the GPR
158 instrument, which recorded position data at every radar sample with RMS values of 3 m. During radar
159 processing we average 75 adjacent traces, corresponding to a distance of ~20 m, so errors in GPS positioning
160 have a negligible effect on the final dataset.

161

2.2. Ground-penetrating radar

We develop a spatially continuous record of accumulation using GPR profiles collected with Geophysical Survey Systems Inc. (GSSI) SIR-3000 (during 2016) and SIR-30 (during 2017) radar units with a 400 MHz antenna (following Hawley et al., 2014). The antenna was towed on the snow surface in a small plastic sled ~5 m behind a wooden Nansen sled and ~15 m behind a snow machine. We recorded 2048 samples (2016) and 4096 samples (2017) per trace over a range window of 800 ns (Figure 2). [At a relative permittivity of \$1.26 \pm 0.07\$, typical of firn in the GrIS percolation zone, the range was ~111–114 m.](#) The 400 MHz short-pulse radar has a range resolution (ability to resolve distinct features) of 0.35 ± 0.1 m in firn, which is fine enough to resolve Internal Reflecting Horizons (IRHs) that have been shown to represent isochrones (Medley et al., 2013; Rodriguez-Morales et al., 2014; Spikes et al., 2004; Hawley et al., 2014). We recorded 10 traces per second, which at the snowmobile’s average travel speed of approximately 2.75 m s^{-1} results in ~3.6 traces recorded per meter. Note that this spacing between traces varies with vehicle speed.



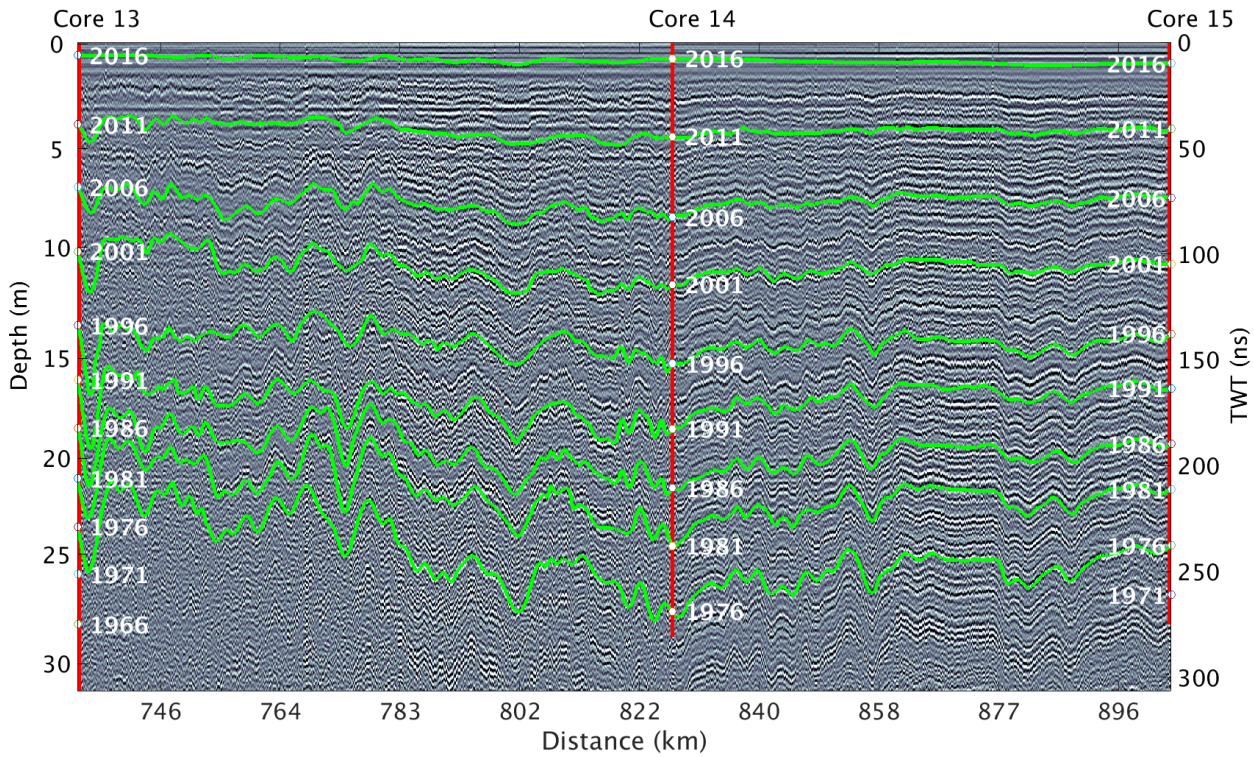


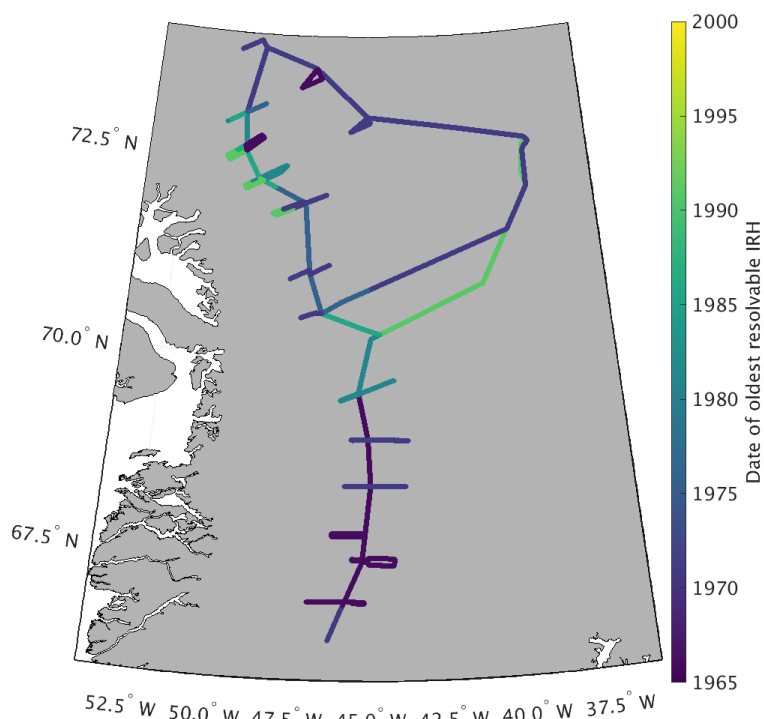
Figure 2. Radargram showing the top 32 m of the transect along the main 2017 traverse from Core 13 to Core 15. Cores are indicated as red lines down to their final depth, with dates plotted every 5 years at corresponding depths. Traced internal reflecting horizons are shown as isochronous green lines. The depth scale on the vertical axis is calculated from the TWT-depth conversion (see Section 2.4) for Core 13, although there is no visual difference in depth scale across this radargram.

Depending on signal attenuation within the firn column, IRHs can be traced to a depth of 20 – 50 m (Figure 2), providing accumulation records over the past 20 – 60 years (Figure 3). For areas with high attenuation (i.e. shallow penetration of the radar signal), such as lower elevation regions with more refrozen melt layers, we calculate accumulation results for shorter time periods. We are not able to trace as many IRHs to the west of Cores 10 – 13 compared to the east due to higher signal attenuation, resulting in slightly different (less than $0.03 \text{ m w.e a}^{-1}$) average accumulation values on either side of these core locations (Figure 3). Likewise, we experienced an equipment malfunction at the end of the 2016 traverse, reducing the number of observable IRHs from Core 7 to Summit Station (Figure 3). We have less confidence in calculated accumulation throughout this section of the traverse due to this malfunction, although the 2017 Summit to Core 8 interval overlaps nicely with the last 140 km of the problematic 2016 interval, and provides high quality accumulation measurements for this section near Summit Station.

We reduce the GPR data volume and signal noise by averaging 75 adjacent traces, which has the effect of suppressing random noise by the principle of trace stacking (Yilmaz, 2001). We apply a combination of median trace filtering, residual mean filtering (Gerlitz et al., 1993), and bandpass filtering using a butterworth design (Selesnick and Sidney Burrus, 1998) between 200 – 800 MHz. For data visualization, we apply an automatic gain control (Yilmaz, 2001) to give the interpreter more confidence when picking IRHs.

197

198



199

200

201

Figure 3: Date of oldest resolvable internal reflecting horizon throughout the entire GreenTrACS traverse route. Anomalous young ages from Core 7 to Summit are due to equipment malfunction.

202

203

2.3. Firn core processing and density profiles

204

205

206

207

208

209

210

211

212

213

214

215

The amount of snow mass and the time span between IRHs are necessary to calculate accumulation rates [from the GPR profiles](#). The accumulation rate is a function of the depth-age scale, travel time-depth conversion rate, and the firn density profile. We obtain the depth-age and depth-density scales from each of the shallow firn cores collected along the GreenTrACS traverse, and from density models based on temperature and accumulation rate data.

The sixteen firn cores were drilled using an Ice Drilling Program hand auger with a Kyne sidewinder attachment (see Graeter et al., 2018). We sampled the firn cores for chemical measurements using a continuous ice core melter system with discrete sampling (Osterberg et al., 2006). We used an Abakus (Klotz) laser particle detector to measure microparticle concentrations and size distribution from the continuous ice core meltwater stream, a Dionex Model ICS5000 capillary ion chromatograph to measure major ion (Na^+ , Mg^{2+} , Ca^{2+} , K^+ , NH_4^+ , Cl^- , NO_3^- , SO_4^{2-}) and methanesulfonic acid concentrations, and a Picarro L1102-I and

216 a Los Gatos Research Liquid Water Isotope Analyzer to measure oxygen and hydrogen isotope ratios ($\delta^{18}\text{O}$,
217 δD ; Graeter et al., 2018).

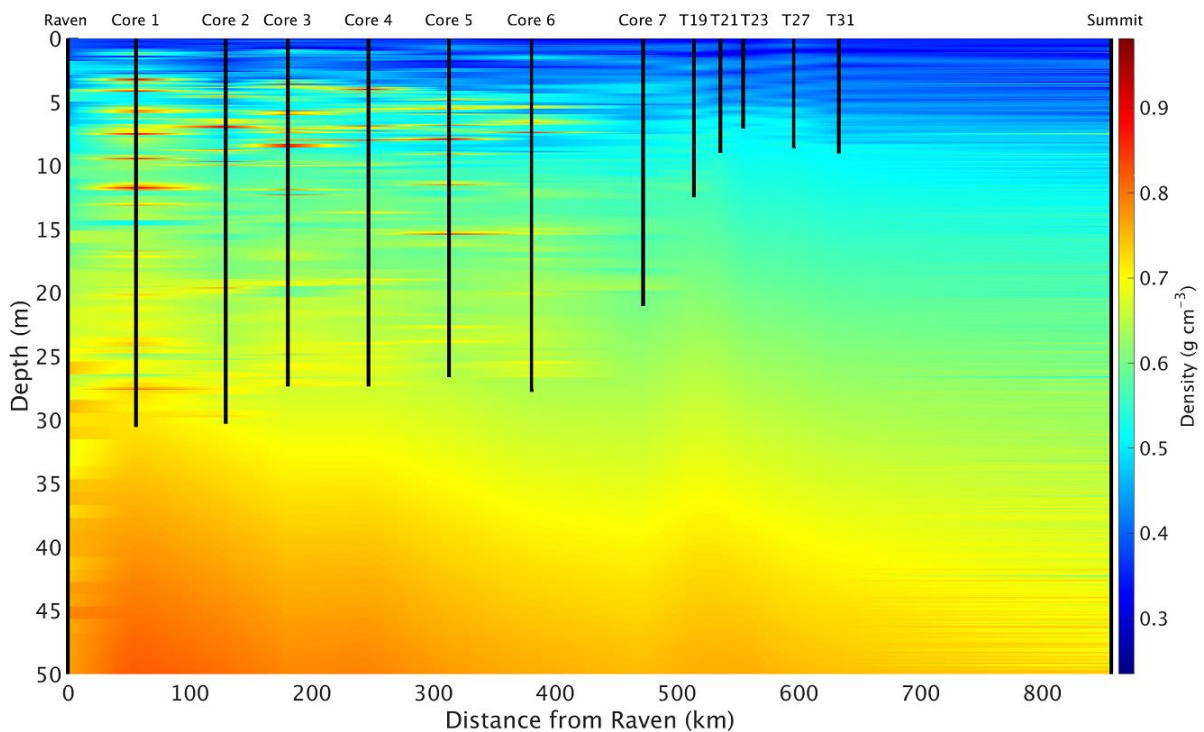
218
241 We determine depth-age curves for each core by identifying annual layers based on seasonal oscillations in
242 $\delta^{18}\text{O}$ and the concentrations of major ions and dust, consistent with previous ice core studies in this region
243 (Graeter et al., 2018; Mosley-Thompson et al., 2001; Osterberg et al., 2015). [While meltwater percolation](#)
244 [smooths the signal of some of these tracers, we can still confidently determine the depth-age curve using](#)
245 [nearly unperturbed oscillations in \$\delta^{18}\text{O}\$ and dust.](#) We combine the depth-age scales with measured density to
246 calculate annual accumulation rates at the firn core sites.

247
248 At each firn core and at the ends of each spur, we measured the density in the top meter of snow using a 1000
249 cm^3 SnowMetrics cutter. To calculate ~~firn core~~-density profiles [from the firn cores](#), we measured the mass,
250 length, and diameter of 0.03–1 m long core segments in the field and again after transporting the cores to the
251 Dartmouth College Ice Core Laboratory. [Additionally, we measured melt layer thickness in the laboratory](#)
252 [following Graeter et al. \(2018\).](#) To calculate accumulation rates at Raven/Dye-2, we use density data from a
253 119.6 m long firn core collected in 1997 (Bales et al., 2009) and a 19.3 m long core collected from the same
254 location in 2015, which did not include accumulation data (Vandecrux et al., 2018). For this location we use
255 the most recent density data for the near-surface and the older densities for depths below the 2015 core.
256 Likewise, we use a density profile from a 109 m long firn core collected from Summit in 2010 (Mary Albert,
257 personal communication, 2015). We also incorporate density data from measurements along the EGIG
258 traverse at T19, T21, T23, T27, and T31 to improve the density profile between Core 7 and Summit (Morris
259 and Wingham, 2014).

260
261 After collecting each firn core, we measured borehole temperature for 24 – 48 hours using a 20 m long
262 thermistor string. We estimate mean annual temperature from the deepest thermistor on the twenty-
263 thermistor-string. [These measurements agree with MODIS satellite derived mean annual temperature \(Hall](#)
264 [et al., 2012\) to within \$\pm 1\$ °C for each firn core location.](#) For the location of each firn core, we use the depth-
265 density data from that core and ~~then~~ calculate a Herron and Langway (1980) depth-density model for depths
266 below the core using our measured mean annual temperature, firn core mean annual accumulation, and top-
267 meter snow density. Likewise, we calculate Herron-Langway profiles for the ends of each spur using MODIS
268 satellite derived mean annual temperature (Hall et al., 2012), MAR modeled accumulation (Burgess et al.,
269 2010), and the measured snow density in the upper meter of each of the spur’s snow pits. Finally, we
270 interpolate depth-density profiles both between firn cores and along radar spurs to estimate the depth-density

271 matrix everywhere along our traverse (Figure 4). Final [calculated](#) accumulation rates are insensitive to the
272 [input](#) accumulation [parameter](#) we use to calculate our Herron-Langway models (Lewis et al., 2017).
273

274 As shown in Figure 4, ice layers within several firn cores are extrapolated laterally along the traverse,
275 although these dense lenses are typically both localized and heterogeneous [in nature at these elevations](#)
276 (Brown et al., 2011; Rennermalm et al., 2013). [This](#) Numerous studies have documented the heterogeneity of
277 [firn throughout the percolation zone and the complications of calculating SMB due to ice pipes and lenses](#)
278 [\(Brown et al., 2011, 2012; De La Peña et al., 2015\)](#). Here we attempt to accurately calculate accumulation
279 [using interpolated firn cores and in situ GPR throughout this complicated](#) region. Our ice lens density
280 interpolation is as accurate as possible between firn cores without additional *in situ* data, and this estimation
281 does not significantly alter our results, as discussed in Section 2.6, since the ice layers represent a small
282 fraction of the total depth to IRHs.



283
284 **Figure 4. Depth-density profile along the main 2016 traverse used for calculation of electromagnetic wave velocity and accumulation in**
285 **this study. Densities are linearly interpolated between the two nearest cores and are modeled using Herron-Langway profiles below the**
286 **depth of each core. The left and right boundary data come from the Raven/Dye-2 and Summit firn cores, respectively. Ice layers in Cores**
287 **1 – 5 are clearly visible as red lenses, but their extent is, in reality, likely more localized.**

288

289 2.4. Travel-time to depth conversion

290 We convert the radar travel time to depth by iteratively multiplying the velocity of the electromagnetic wave
291 by the signal's one-way travel time to each IRH. The electromagnetic speed of the radar wave, v (m s^{-1}), is

322 calculated from the [relative](#) dielectric permittivity, ϵ_r (dimensionless), and the speed of light in a vacuum, c
323 ($3 \times 10^8 \text{ m s}^{-1}$), from

$$324 \quad v = \frac{c}{\sqrt{\epsilon_r}} \quad (1).$$

325 In turn, we calculate the [relative](#) dielectric permittivity ~~for each radar trace~~ from the density, ρ (g cm^{-3}), of
326 snow and ice at depth, as shown in [Figure 4](#)~~Figure 4~~, for each radar trace at every range bin (following Kovacs
327 et al., 1995) by

$$328 \quad \epsilon_r = (1.0 + 0.845 * \rho)^2 \quad (2).$$

329 We calculate the depth of each subsequent radar sample for each trace in the profile using the radar travel
330 time and velocity profile from equations 1 and 2, following Hawley et al. (2014) and Lewis et al. (2017).

332 **2.5. Internal reflecting horizons**

333 We manually select 10 clear, strong IRHs spaced approximately 5 years apart to consistently trace from
334 Raven/Dye-2 to Summit Station and throughout the 2017 main traverse (Figure 2). We trace each layer
335 manually by visually identifying strong amplitude peaks throughout the radargram, starting with the 2016
336 layer and working downwards. We use a spline interpolation between manual picks to trace each layer along
337 large amplitude reflections every $\sim 500 - 700 \text{ m}$ along the traverse. When a layer appears to bifurcate due to
338 changes in accumulation, we continue to trace the layer based on the trajectory of surrounding IRHs.
339 ~~Horizons are not traced in areas where the attenuated signal makes them too difficult to interpret~~ Each horizon
340 is traced throughout the traverse, except in areas where the attenuated signal makes it too difficult to interpret
341 (Figure 3)~~Figure 3~~). We trace layers for each spur starting at the depth of each layer at the corresponding firn
342 core location. We can trace layers below the depth of some firn cores by tracing them from cores that are
343 deeper or have lower accumulation rates.

344
345 We trace layers between cores using a connect-the-dots approach using the depth-age scale at each firn core.
346 We trace layers from one firn core to the next before checking that we intersect that core location at the
347 proper depth for the age of our traced IRH. Note that the depths of several layers at Cores 2 – 16 are located
348 below the bottom depth of those cores. Since these layers are isochronous, they are used to calculate
349 accumulation over appropriate time epochs by using dates obtained from intersections with other cores (see
350 [Figure 3](#)~~Figure 3~~).

2.6. Accumulation calculations and uncertainty

Finally, we calculate snow accumulation using the firn core depth-age scales, measured and interpolated depth-density profiles (Figure 4), and traced IRHs (Figure 2). We calculate the water equivalent accumulation \dot{b} (m w.e. a^{-1}) between adjacent IRHs from the depth z (m) and age t (year) of each layer, the average density ρ (kg m^{-3}) between layers, and the density of water ρ_w (1000 kg m^{-3}):

$$\dot{b} = \frac{1}{t_2 - t_1} \int_{z_1}^{z_2} \frac{\rho(z)}{\rho_w} dz \quad (3).$$

We correct for layer thinning using a Nye (1963) model. The thinning factor has an average value of 0.9993 ± 0.0003 and is multiplied by the accumulation rate for each radar trace. For each radar trace, the thinning factor, $\lambda(z)$, is calculated from the average accumulation \dot{b} (m w.e. a^{-1}) of each epoch, average age of the epoch a (year), and water equivalent thickness of the GrIS H (m), from Morlighem et al. (2014):

$$\lambda(z) = e^{-\frac{b}{H} a} \quad (4).$$

Accumulation uncertainty can arise from independent errors in tracing IRHs, errors from incorrectly dating firn cores, and/or errors in the densities used for converting from separation distance to water equivalent accumulation. To reduce tracing errors, we retraced each IRH along the two main traverse paths four times ~~each piece~~. Close inspection of the IRHs reveals that the peaks defining IRHs are within ± 2 radar samples (within at most ± 0.12 m), and incorrectly jumping to the next IRH would result in an error of at most ± 10 samples (within ± 0.55 m). ~~We chose an~~ ~~Our average~~ epoch between IRHs ~~of~~ ~~is~~ 5.0 years from the firn core ~~chemistry~~ depth-age scales, which corresponds to a maximum tracing error of $\sim \pm 0.11$ m a^{-1} for each epoch, or a maximum error of ± 0.061 m w.e. a^{-1} , ~~for given~~ an average ~~firm~~ density of 0.55 g cm^{-3} ~~over across~~ this dataset.

We perform a leave-one-out cross validation to calculate accumulation errors at locations where we do not have firn core density profiles. Here we choose one of the sixteen firn cores, in addition to the Raven/Dye-2 and Summit cores, to omit from our density interpolation (Figure 4), so that we interpolate density profiles between adjacent firn cores and a Herron-Langway profile at the missing core location. We find maximum single-epoch errors of 0.079 m w.e. a^{-1} and maximum RMS (1971 – 2016) errors of 0.046 m w.e. a^{-1} (Table 1) at the location of missing cores, ~~corresponding to 20.1% of the accumulation at that location.~~ These differences are approximately twice as large at Cores 1 – 6 than Cores 7 – 16 due to larger differences between measured and interpolated density profiles, likely a result of meltwater percolation and ice lenses (Graeter et al., 2018).

385 Similarly, we perform a leave-out-out validation by omitting a firn core density profile location entirely and
 386 interpolating density profiles over a larger distance (e.g. between Core 1 and Core 3). In this case we find
 387 maximum single-epoch errors of 0.057 m w.e. a⁻¹ and maximum RMS (1971 – 2016) errors of 0.033 m w.e.
 388 a⁻¹. Throughout this study, we use our measured density profiles to calculate accumulation at core locations,
 389 rather than rely on Herron-Langway density models that would result in larger uncertainties.
 390
 391

392 We conservatively take our accumulation error from missing density measurements to be 0.079 m w.e. a⁻¹.
 393 This error highlights the importance of our firn core spacing between 40 – 100 km along the traverse and
 394 confirms that the accuracy of future remotely sensed radar accumulation (e.g. IceBridge snow and
 395 accumulation radars) estimates depend on precise field-based *in situ* density profiles for accurate
 396 accumulation history in the percolation zone. Overly et al. (2016) calculated accumulation in the dry snow
 397 zone using Herron-Langway profiles within 3.5% of accumulation calculated using neutron-probe density
 398 profiles. However, here we show that *in situ* measurements, or accurate meltwater percolation modeling
 399 (Meyer and Hewitt, 2017), are required to correctly calculate SMB in the percolation zone.
 400

401 **Table 1. Difference between accumulation rates at each GreenTrACS core site calculated using Herron-Langway profiles and firn core**
 402 **density information.**

Core	RMS average difference (m w.e. a ⁻¹)	Max epoch difference (m w.e. a ⁻¹)	Max Epoch difference (% of acc.)
1	0.046	0.079	20.1
2	0.025	0.061	16.2
3	0.037	0.074	19.9
4	0.028	0.045	10.7
5	0.026	0.054	11.5
6	0.038	0.052	10.0
7	0.015	0.026	5.4
8	0.026	0.045	10.3
9	0.030	0.049	10.9
10	0.019	0.039	8.5
11	0.023	0.035	5.0
12	0.018	0.027	8.2
13	0.025	0.031	10.7
14	0.019	0.027	8.2
15	0.010	0.016	5.3
16	0.014	0.025	8.2

403

We assume uncertainty in dating the firn cores from annual [layer counting variations in chemistry](#) to be ± 0.5 years (Buchardt et al., 2012). At the lowest accumulation locations, the smallest distance between layers is 0.15 m w.e. over an epoch of 4.91 years. This gives an uncertainty in accumulation due to dating of at most $\sim \pm 0.03$ m w.e. a^{-1} . The error associated with measuring *in situ* firn density has been estimated to be 1.4% (Karlöf et al., 2005). However, following Hawley et al. (2014) and Lewis et al. (2017), we conservatively assume that our measurements have a density measurement error of up to twice this large, corresponding to a maximum accumulation error of ± 0.014 m w.e. a^{-1} .

We calculate the total uncertainty from formal error propagation (following Bevington and Robinson, 1992) from the average accumulation rate $\dot{b} = 0.385$ m w.e. a^{-1} , average thickness between IRHs $\Delta h = 3.56$, uncertainty in tracing δh , average firn density ρ , uncertainty in density measurements $\delta \rho$, average time period between IRHs Δt , and uncertainty in core dating δt . We find [the](#) total accumulation rate uncertainty [for each epoch to be](#) 0.0709 m w.e. a^{-1} from equation 5.

$$\sigma_{\dot{b}} = \sqrt{\dot{b}^2 \left(\left(\frac{\delta h}{\Delta h} \right)^2 + \left(\frac{\delta t}{\Delta t} \right)^2 + \left(\frac{\delta \rho}{\rho} \right)^2 \right)} \sigma_{epoch} = \sqrt{\dot{b}^2 \left(\left(\frac{\delta h}{\Delta h} \right)^2 + \left(\frac{\delta t}{\Delta t} \right)^2 + \left(\frac{\delta \rho}{\rho} \right)^2 \right)} \quad (5)$$

Due to the random and non-systematic nature of these errors, we can assume that they are unlikely to contribute to a regional or temporal accumulation bias. To calculate uncertainty for accumulation averaged over multiple epochs ($\sigma_{n\text{-epochs}}$) we divide our uncertainty σ_{epoch} by the square root of the number of traced layers (n) at that location.

$$\sigma_{n\text{-epochs}} = \frac{\sigma_{epoch}}{\sqrt{n}} \quad (6).$$

2.7. Model comparison

We compare our GreenTrACS accumulation results with annual outputs from Box et al. (2013; hereafter “Box13”; 1840 – 1999), the Fifth Generation Mesoscale Model (Polar MM5; 1958 – 2008; Burgess et al., 2010), MAR (1948 – 2015; Fettweis et al., 2016), and the Regional Atmospheric Climate Model (RACMO2; 1958 – 2015; Noël et al., 2018) over common time periods. Grid cell sizes for these model outputs are 5 km, 3 km, 5 km, and 1 km, respectively. For each radar trace we calculate statistically significant differences (at $\alpha = 0.05$) using a two sample t-test with the GreenTrACS accumulation records for each epoch and RCM accumulation for each common year. Additionally, we compare our GreenTrACS accumulation with an accumulation map kriged from 295 firn cores and 20 coastal weather stations (Bales et al., 2009; hereafter “Bales09”). We perform the same two sample t-test with the reported Bales09 uncertainty of 0.092 m w.e. a^{-1} (Bales et al., 2009).

437 **2.8. Accumulation trends**

438 To investigate recent changes in GrIS accumulation, we calculate trends in accumulation across our GPR and
439 GreenTrACS firn core dataset. We fit a linear model to the accumulation time series for each radar trace and
440 analyze the trend for both slope and statistical significance. Likewise, we calculate trends and their statistical
441 significance for total precipitation (snowfall + rainfall) for MAR and RACMO2 grid cells from 1996 through
442 the end of both models' temporal coverage. We can compare these results with our accumulation trends since
443 precipitation and accumulation are nearly identical above the equilibrium line altitude, due to zero runoff and
444 negligible sublimation within the percolation zone.

445 **2.9. Storm track changes**

446 To investigate the potential role of changing storm tracks in precipitation changes over the Western GrIS, we
447 utilize the updated Serreze (2009) storm track database. This database contains six-hour interval positions of
448 extratropical cyclone storm centers on a 2.5° grid. These centers are defined when a gridpoint sea level
449 pressure is surrounded by gridpoints at least 2 mb higher than the central point (Serreze, 2009). We calculate
450 the total number of days in which a storm center is located within our region of interest for each season. To
451 determine statistical significance, we run a two sample t-test on the number of storms in our region of interest
452 between 1958 – 1996 compared with 1996 – 2016.

453 **3. Results and discussion**

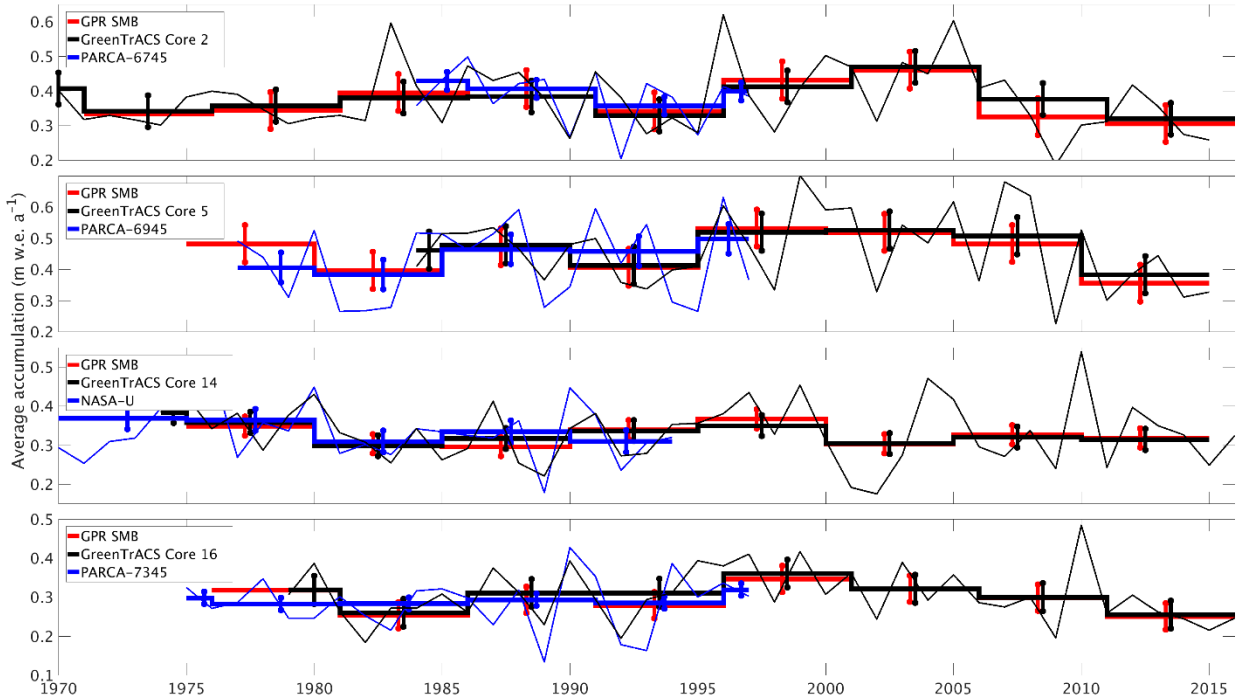
454 **3.1. Firn core and GPR accumulation records**

455 Figure 1 displays the mean accumulation at each location along the traverse route, with higher accumulation
456 rates in the southwest and lower accumulation rates at higher elevations of the ice sheet interior, broadly
457 consistent with previously published accumulation compilations (e.g. Bales et al., 2009) and RCM output
458 (Box et al., 2013; Burgess et al., 2010; Fettweis et al., 2016; Noël et al., 2018). We analyze localized
459 differences between GPR derived accumulation and these RCMs in Section 3.3. There is an especially high
460 accumulation zone near Core 11 ($0.685 \text{ m w.e. a}^{-1}$), nearly double the accumulation at Core 10 (0.453 m w.e.
461 a^{-1}) and Core 12 ($0.327 \text{ m w.e. a}^{-1}$), respectively situated only 43 km northwest and 73 km southwest of Core
462 11. In the GPR data, the number of traceable IRHs is highest towards the interior of the ice sheet and lowest
463 in warmer areas towards the coast and in the south, where refrozen percolated melt water from enhanced
464 surface melt attenuates the radar signal and reduces the number of observable IRHs (Brown et al., 2011;
465 [Figure 3](#)Figure-3).

466 **3.2. Validation with past measurements**

467 We validate our accumulation record with published core records from the PARCA campaign and
468 accumulation data from the NASA IceBridge program. The locations of GreenTrACS Core sites 2, 5, 9, 10,
469 11, 14, 15, and 16 were chosen to reoccupy PARCA core locations 6745, 6945, 7147, 7247, 7249, NASA-
470 U, 7347, and 7345, respectively. These GreenTrACS cores overlap with the accumulation history of each
471 PARCA core and extend the record from 1997/1998 to 2016/2017. Accumulation rates derived from
472 GreenTrACS firn cores are within error of those determined from corresponding PARCA cores during the
473 period of overlap. Figure 5 compares the accumulation records from PARCA sites 6745, 6945, 7345, and
474 NASA-U to their corresponding GreenTrACS cores, demonstrating that each pair of cores has similar long-
475 term mean accumulation and nearly identical decadal variability. Thus, we have confidence in firn core
476 derived accumulation rates that are used in subsequent GPR calculations of accumulation rates throughout
477 the GreenTrACS traverse.

478



479

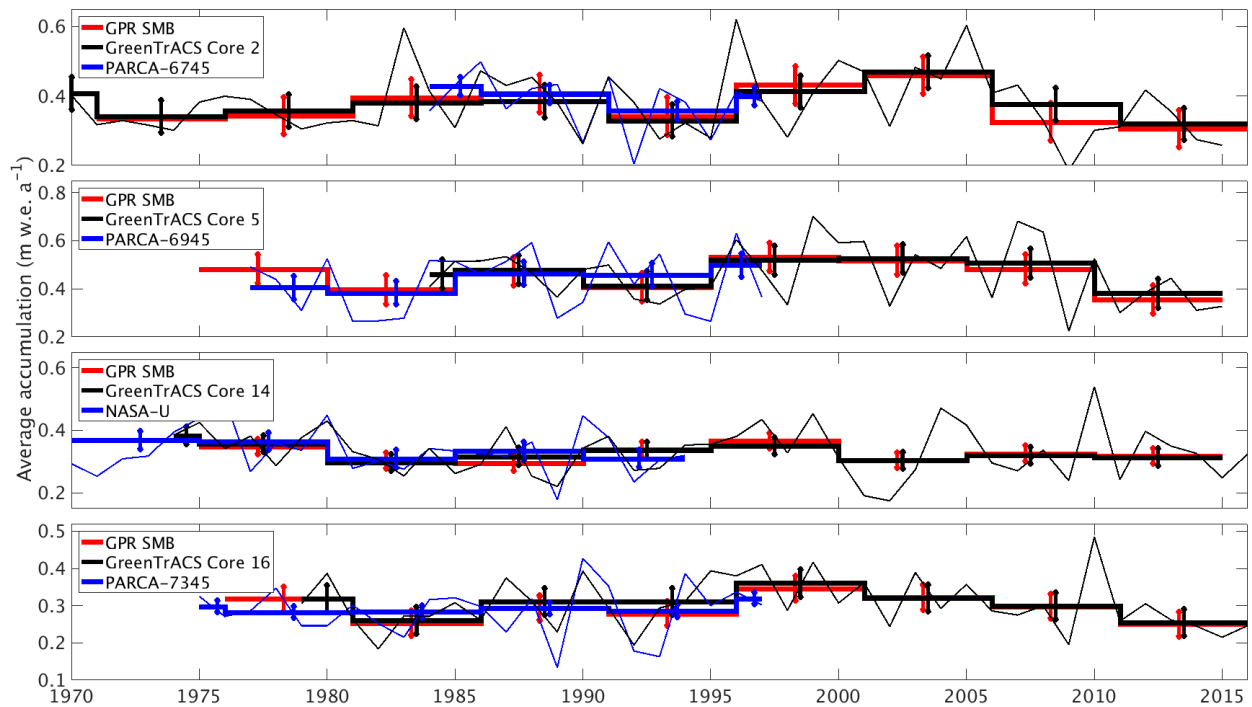


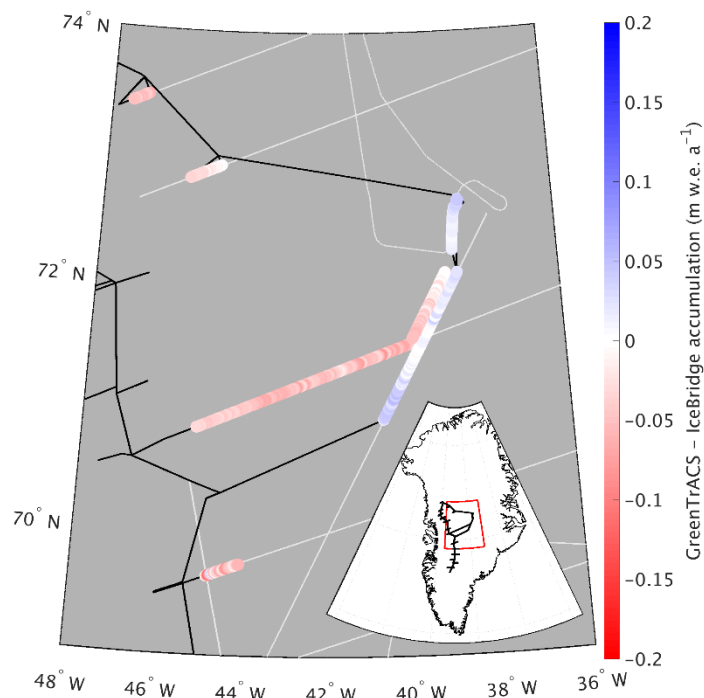
Figure 5. Accumulation from GPR and collected firn cores (this study) compared with cores from the PARCA Campaign. Thin lines represent annual PARCA (blue) and GreenTrACS (black) firn core accumulation, while thick lines are 5-year averages over corresponding GPR epochs. Error bars represent one standard deviation over each epoch. GPR and PARCA accumulation averages and decadal trends are statistically indistinguishable.

Average (1966 – 2016) GPR accumulation is statistically indistinguishable with average (1962 – 2014) IceBridge Accumulation Radar measurements analyzed by Lewis et al. (2017), with an RMS difference of 0.0387 ± 0.0327 m w.e. a^{-1} along a total of 562.5 km of overlap (Figure 6). The disagreement is largest at lower elevations, where Herron and Langway (1980) density profiles used in Lewis et al. (2017) differ the most from GreenTrACS firn core density profiles in the upper 30 m of firn, demonstrating the importance of field observations for calibration and validation. The close agreement at higher elevations is illustrated in Figure 7a, where our GreenTrACS accumulation measurements are statistically indistinguishable from the IceBridge radar-derived accumulation (Lewis et al., 2017) along the 285 km A – A’ transect on Error! Reference source not found. Figure 1. Notice that the uncertainty in GreenTrACS accumulation progressively decreases higher in the percolation zone and into the dry snow zone (towards the right in Figure 7) along this transect as density becomes less heterogeneous from fewer melt layers (Graeter et al., 2018) and IRHs become easier to trace.

Similarly, our 2011-2016 accumulation is statistically indistinguishable from average 2009 – 2012 IceBridge snow radar measurements analyzed by Koenig et al. (2016), with an RMS difference of 0.0489 ± 0.0961 m

\$01
\$02
\$03
\$04
505

w.e. a⁻¹ along a total of 69.7 km of overlap (not shown). Koenig et al. (2016) use a different radar system on an airborne platform and are able to calculate annual accumulation at elevations below 2000 m a.s.l., however the GreenTrACS accumulation record covers a longer temporal duration than the data from that study.



506
507
508
509
510

Figure 6. Difference between averaged (1966 – 2016) GreenTrACS accumulation and average (1962 – 2014) IceBridge Accumulation Radar rates from Lewis et al. (2017) across all 562.5 km of overlap. Spatially overlapping section of 2016 and 2017 traverses displayed as adjacent tracks. Also showing extent of GreenTrACS traverse (black) and IceBridge accumulation radar (grey). Inset shows map location with respect to GreenTrACS traverse (black).

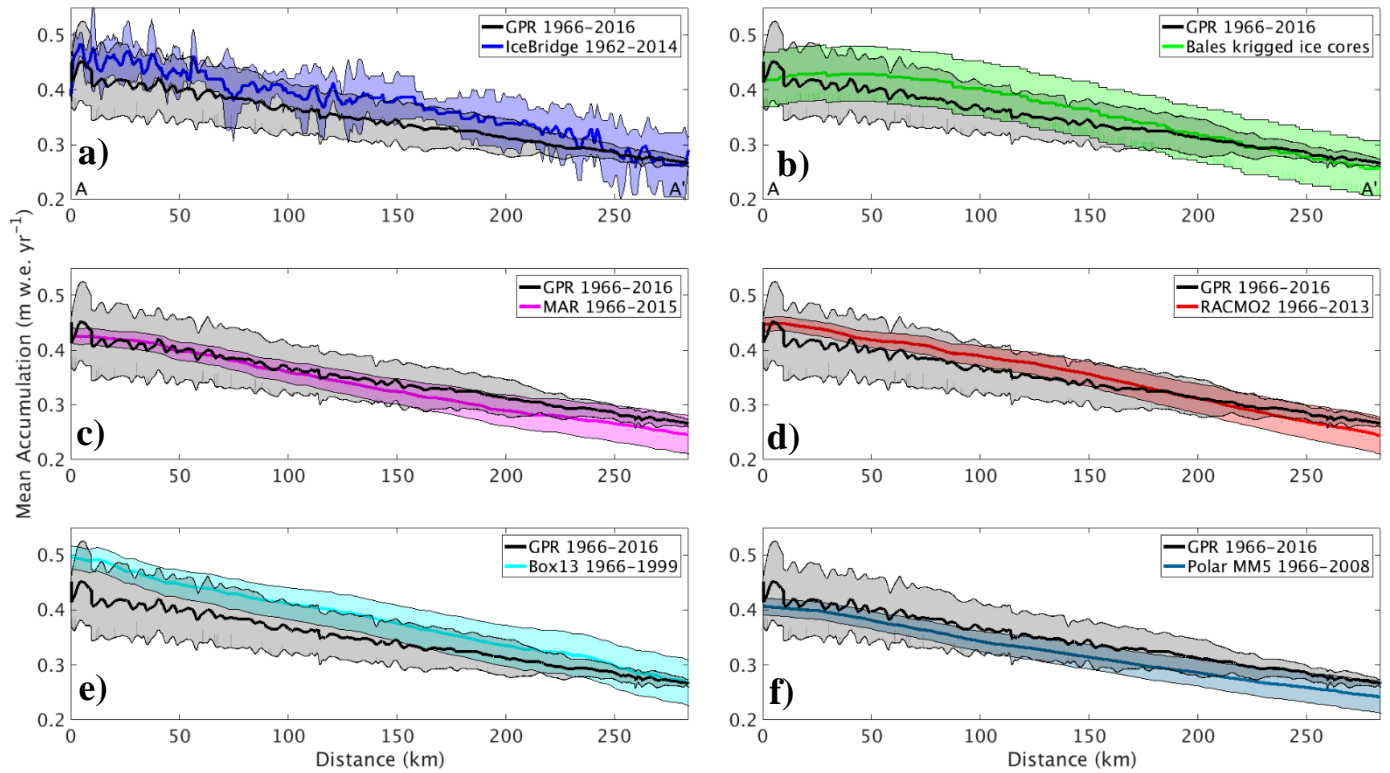
511

3.3. Comparison to modelled accumulation

512
513
514
515
516
517
518
519
520
521
522

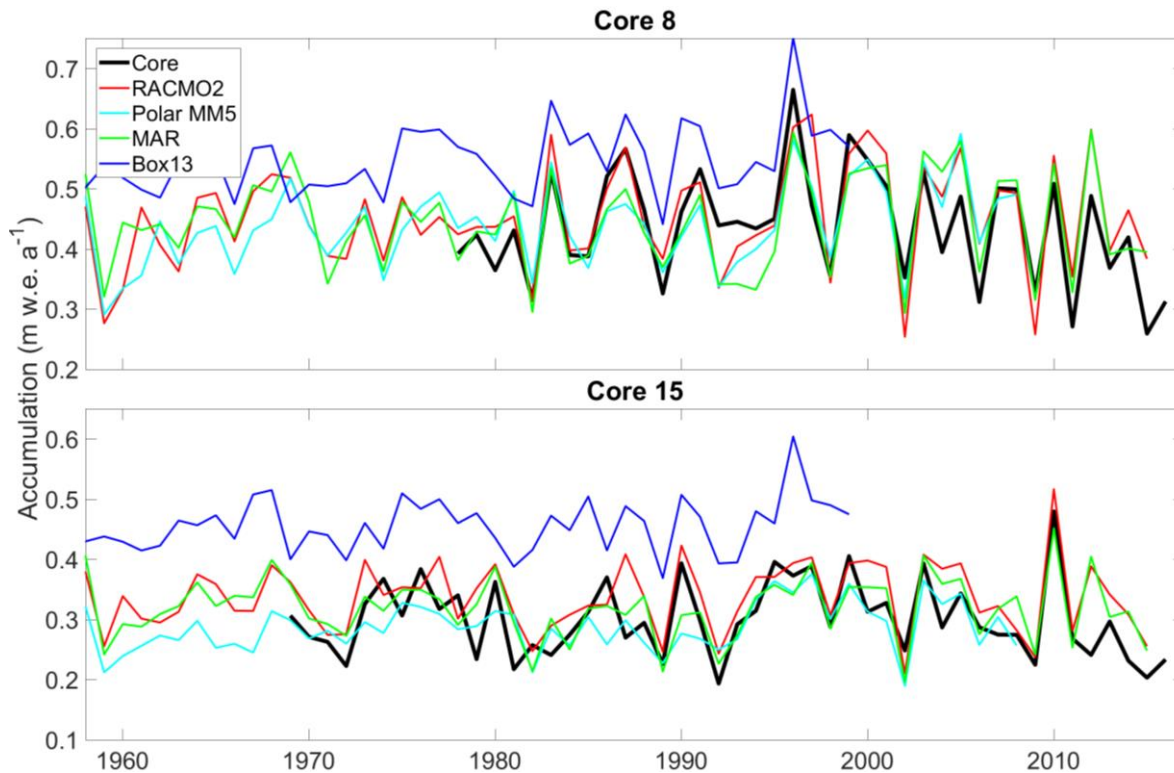
We assess differences between RCM accumulation output and GreenTrACS accumulation record at each firn core site, two of which are shown in Figure 8. In general, year-to-year correlations between GreenTrACS firn core accumulation records and RCM output for the corresponding grid cell are strong, positive, and statistically significant (Table 2). On average, GreenTrACS firn cores' correlation coefficient with MAR output is 0.718, with PolarMM5 is 0.701, with Box13 is 0.607, and with RACMO2 is 0.763. Every correlation is statistically significant at $p < 0.05$ except for Cores 7 and 11 with Box13. We do not report a correlation coefficient for Core 11 and Box13 because they only share two common years. Temporal correlation coefficients remain high even at locations with large magnitude differences between RCM output and firn core accumulation. For example, the Box13 model overestimates accumulation at Core 15 by 0.15 ± 0.05 m w.e. a⁻¹, on average, but the model output has a correlation coefficient of 0.48 with Core 15 (Table 2) and

523 matches years of high accumulation (e.g. 1987, 1990, and 1996) and low accumulation (e.g. 1981, 1989,
 524 1992).



525
 526 **Figure 7. Average GreenTrACS GPR accumulation (black) compared with a) IceBridge accumulation radar, b) Bales09 krigged ice core**
 527 **map, c) MAR, d) RACMO2, e) Box13, and f) Polar MM5. GPR measurements are statistically indistinguishable from each of the other**
 528 **measurements along this 285 km transect in the dry snow zone (A – A' on [Error! Reference source not found.](#) Figure 1).**

529



530

531 **Figure 8. Accumulation record at GreenTrACS Core 8 and Core 15 (black) compared with RCM output from RACMO2 (red), Polar**
 532 **MM5 (cyan), MAR (green), and Box13 (blue). We find statistically significant Pearson correlation coefficients between GreenTrACS**
 533 **and RCM accumulation rates for these cores (see Table 2).**

534

535 **Table 2. Pearson correlation coefficients between accumulation rate time series from firn cores and co-located RCM output over their**
 536 **common time period[#].**

	Available data period	MAR	PolarMM5	Box13	RACMO2
Core1	1966 – 2016	0.70	0.66	0.56	0.73
Core2	1969 – 2016	0.75	0.77	0.62	0.79
Core3	1971 – 2016	0.72	0.69	0.63	0.74
Core4	1977 – 2016	0.79	0.74	0.72	0.72
Core5	1984 – 2016	0.81	0.80	0.60	0.79
Core6	1985 – 2016	0.76	0.76	0.65	0.83
Core7	1993 – 2016	0.81	0.82	0.61	0.73
Core8	1978 – 2017	0.78	0.77	0.69	0.81
Core9	1984 – 2017	0.68	0.75	0.74	0.79
Core10	1984 – 2017	0.88	0.80	0.80	0.80
Core11	1997 – 2017	0.75	0.59	N/A	0.75
Core12	1962 – 2017	0.6	0.54	0.53	0.64
Core13	1955 – 2017	0.51	0.62	0.37	0.76
Core14	1974 – 2017	0.70	0.62	0.46	0.74
Core15	1969 – 2017	0.68	0.63	0.48	0.75
Core16	1979 – 2017	0.79	0.77	0.66	0.88

537 [#]Statistically significant correlations ($p < 0.05$) are bold

538

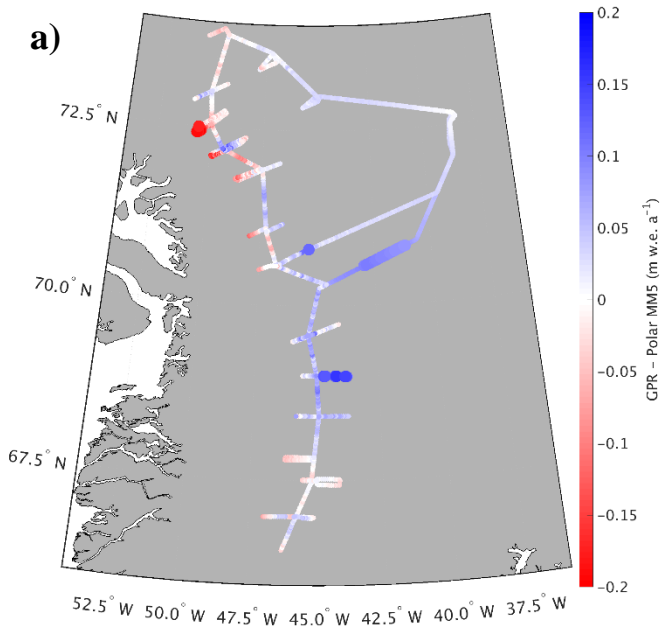
539 We also assess spatial differences between GreenTrACS accumulation and mean RCM accumulation
 540 averaged over several decades. (Table 2). Figure 9 shows that differences between GreenTrACS
 541 accumulation and RCM output increase in magnitude, become more spatially heterogeneous, and vary by
 542 model at lower elevations of the ice sheet where topographic variations are larger and surface melt increases.
 543 Averaged over all 4436 km of the traverse, the RMS difference ($\pm 1\sigma$) between each model and GreenTrACS
 544 accumulation over corresponding data periods (Table 2) is 0.068 ± 0.065 (MAR), 0.0562 ± 0.0548
 545 (RACMO2), 0.0822 ± 0.0702 (Box13), 0.048 ± 0.045 (Polar MM5), and 0.0475 ± 0.0445 m w.e. a^{-1}
 546 (Bales09). We find that RCM differences from GreenTrACS accumulation are small in the dry snow zone
 547 (Figure 9). For example, Figure 7 shows that average GreenTrACS accumulation measurements from 1966
 548 – 2016 along the A – A’ transect in Error! Reference source not found.Figure 4 are statistically
 549 indistinguishable from those derived from the Bales09 krigged ice core map (Figure 7b), MAR (1966 – 2015;
 550 Figure 7c), RACMO2 (1966 – 2013; Figure 7d), Box13 (1966 – 1999; Figure 7e), and Polar MM5 (1966 –
 551 2008; Figure 7f).

552

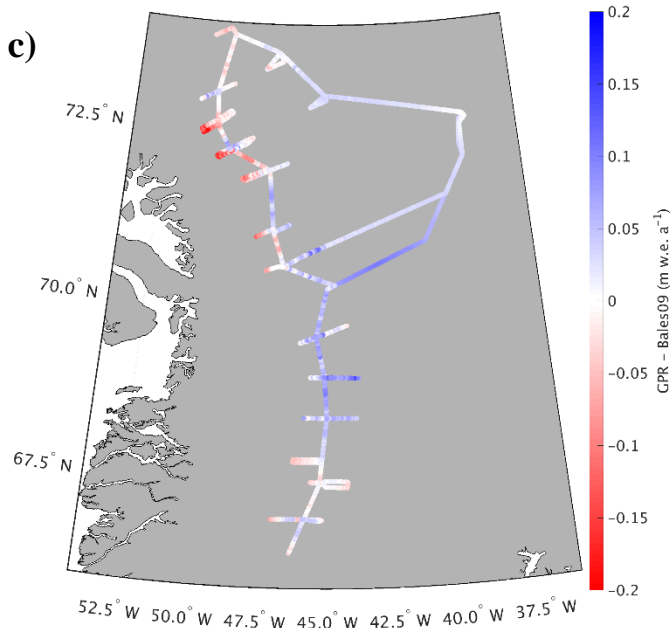
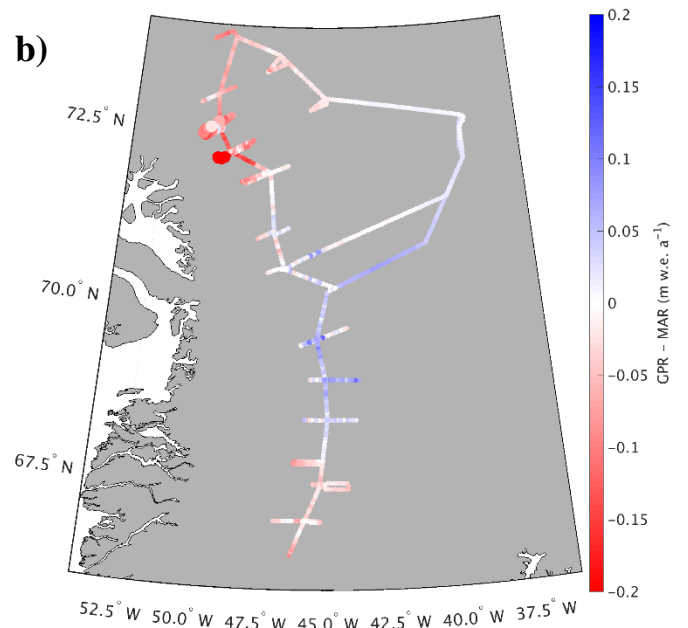
553 However, the high spatial resolution of our dataset shows significant accumulation variability not captured
 554 in model output (Figure 9). For example, Polar MM5 and MAR both underestimate accumulation between

555 Core 4 and Summit, while overestimating accumulation to the west of Cores 10 – 12. Likewise, RACMO2
556 overestimates accumulation between Raven/Dye-2 and Core 5 by 0.03 to 0.08 m w.e. a⁻¹ and shows
557 statistically significant differences east of Cores 11 and 12. Bales09 accurately calculates accumulation along
558 most of the 2016 traverse, but overestimates accumulation west of Cores 11 and 12 by 0.135 ± 0.041 m w.e.
559 a⁻¹. Finally, Box13 overestimates accumulation along many of the western spurs and has statistically
560 significant overestimations of 0.1 to 0.4 m w.e. a⁻¹ between Cores 10 and 16. Box13 overestimates 67.8% of
561 the data in the Core 10 – 16 region by at least 0.1 m w.e. a⁻¹, and 6.6% of that data by at least 0.2 m w.e. a⁻¹.
562

563 Our study is almost entirely contained within drainage basin E from Vernon et al. (2013), who note that basin
564 E is the only major Greenland drainage basin with no statistically significant differences in SMB between
565 the four RCMs. However, differences of 0.1 to 0.4 m w.e. a⁻¹ exist when we look at a local (sub-drainage-
566 basin) scale for each model. All four of the RCMs overestimate accumulation along the western spur of Core
567 11 and they all underestimate accumulation along the eastern spur of Core 5 (Figure 9).
568

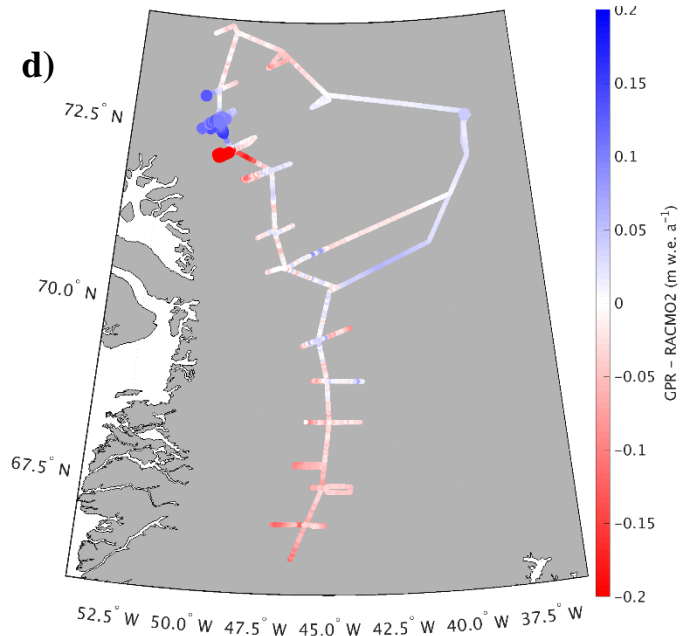


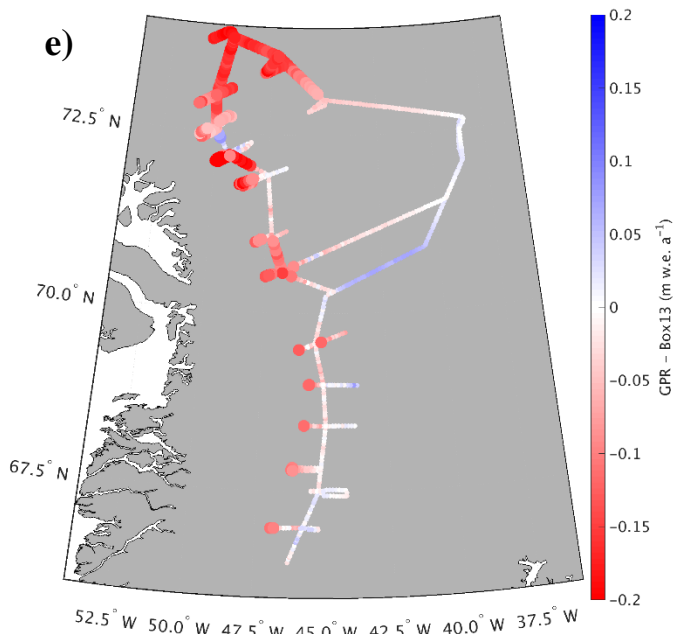
569



570

571





572

573 **Figure 9. Differences between GreenTrACS accumulation and a) Polar MM5, b) MAR, c) Bales09, d) RACMO2, and e) Box13**
 574 **accumulation averaged over the corresponding time periods. Large dots show statistically significant differences from GreenTrACS**
 575 **accumulation.**

576

577 In summary, the RCMs do an excellent job of calculating accumulation averaged over this drainage basin,
 578 with RMS values between 0.048 and 0.0822 m w.e. a⁻¹, but there are larger differences of 0.1 to 0.4 m w.e.
 579 a⁻¹ between model and GPR accumulation on local scales. Differences between GreenTrACS and RCM
 580 accumulation are largest in areas concurrent with the fewest, shortest, and/or most outdated *in situ*
 581 measurements. For example, the GPR vs. model differences near Cores 11, 12, and 13 are relatively large for
 582 all RCMs, despite Core 11 being co-located with PARCA 7249. However, the PARCA cores were collected
 583 over 20 years ago, and Core 11 only spanned 7 years because of the high accumulation rate at that site. This
 584 highlights the importance of collecting updated field-based measurements to calibrate remotely sensed data
 585 and RCM output.

586

587 3.4. Accumulation temporal trends

588 In most locations, there are no statistically significant trends in the GreenTrACS accumulation record from
 589 1966 through the mid-1990s. However, a changepoint analysis (Lavielle, 2005) reveals that accumulation in
 590 the Western GrIS percolation zone changed significantly after the 1995 – 1996 accumulation year. Since
 591 1996, our record indicates a statistically significant average accumulation decrease of 0.009 ± 0.005 m w.e
 592 a⁻², or 2.4 ± 1.5 % a⁻¹, from 1996 to 2017. Although we observe fewer statistically significant accumulation
 593 trends when we expand this analysis to include the entire temporal duration for each firn core, the sign of the
 594 trend at each core site does not change.

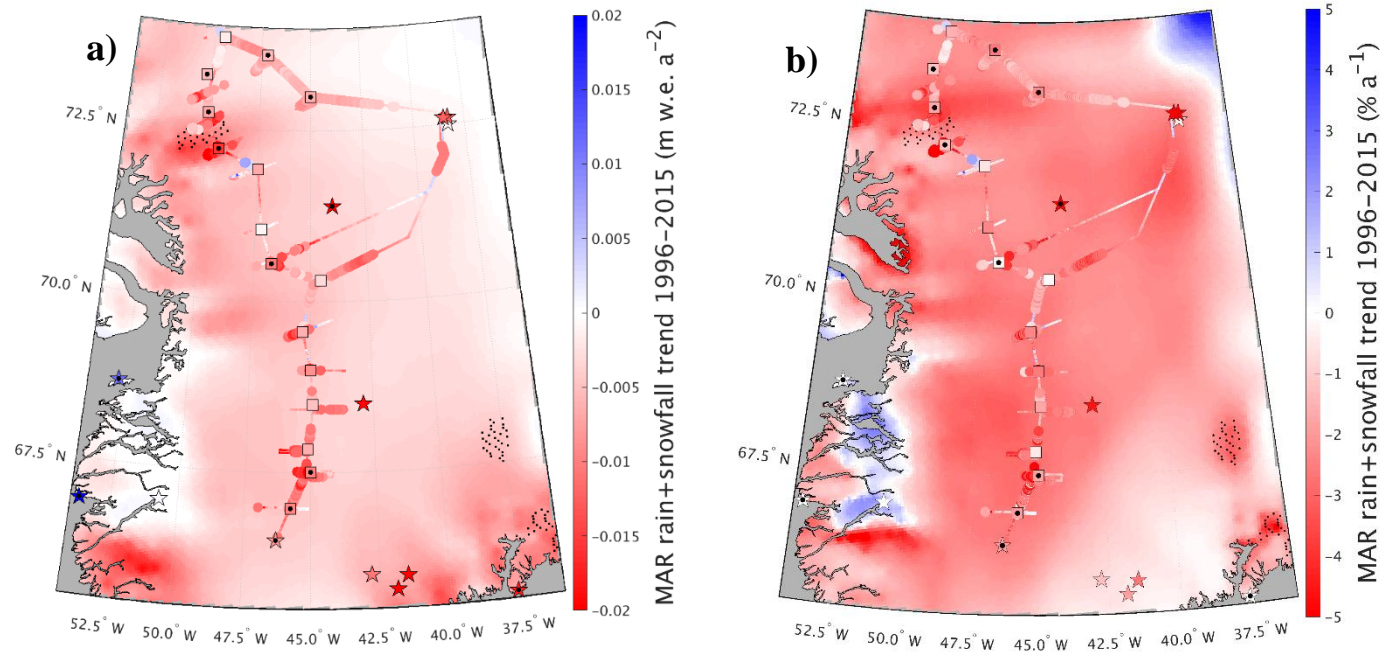
595

596 In Figure 10, we compare the negative accumulation trend in the GreenTrACS record (1996 – 2016) to best-
597 fit linear trends in total precipitation (rain + snowfall) across the ice sheet in MAR and RACMO2 simulations
598 over the 1996 – 2015 and 1996 – 2013 periods, respectively. Also shown in Figure 10 are 1996 – 2016
599 accumulation trends for all 16 GreenTrACS firn cores (squares), accumulation trends from ACT10A (1996
600 – 2010), ACT10B (1996 – 2010), ACT10C (1996 – 2010), D4 (1991 – 2002), D5 (1991 – 2002), Katie (1991
601 – 2002), Sandy (1991 – 2002), and Summit 2010 (1991 – 2010) ice/firn cores (stars on ice sheet), and
602 precipitation trends from coastal weather stations (Mernild et al., 2014; stars on coast). Statistically
603 significant trends ($p < 0.05$) in core data are indicated by black dots, while statistically significant trends in
604 the MAR and RACMO2 output are stippled in black.

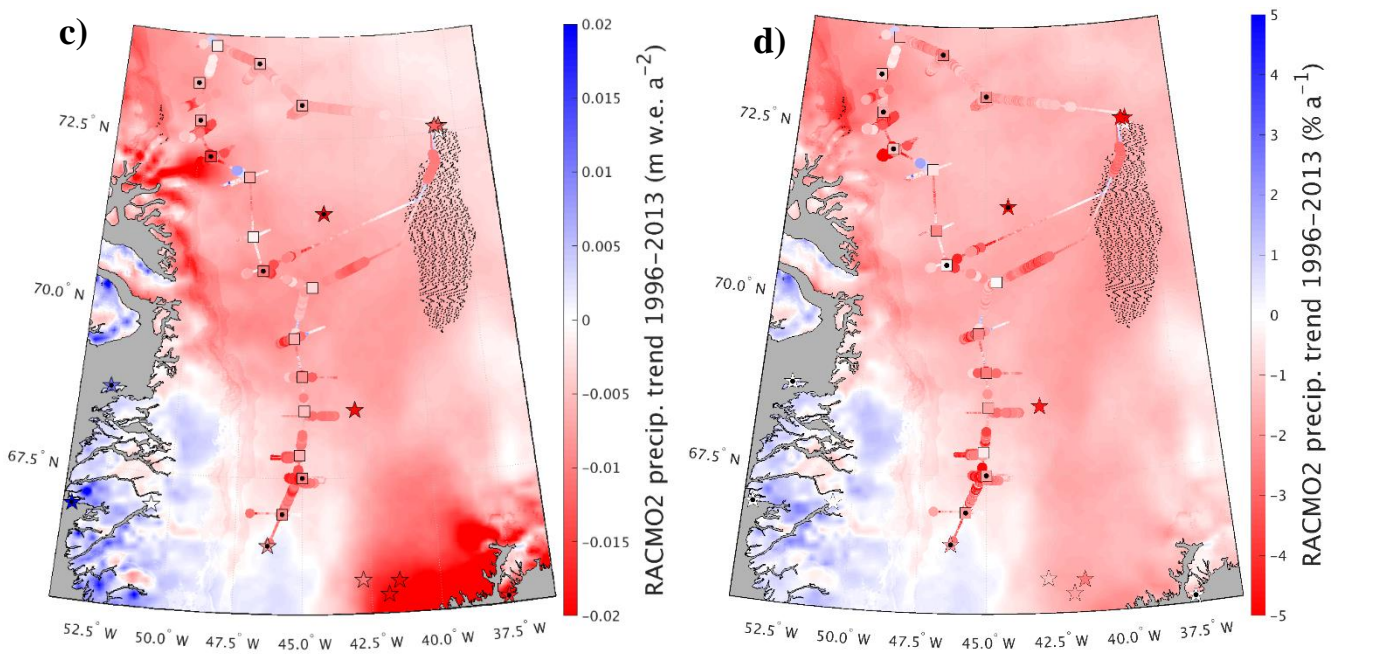
605

606 We find strong agreement between the accumulation decrease in the GreenTrACS record and widespread
607 precipitation decreases in the RCMs over the study area (Figure 10). On average, the RCMs have a more
608 negative precipitation trend than the GreenTrACS record by 0.003 ± 0.005 for MAR and 0.0016 ± 0.0051 m
609 w.e. a^{-2} for RACMO2. Vernon et al. (2013) show a melt-driven decrease in SMB across this drainage basin
610 of 31.1% (ECMWFd), 61.6% (RACMO2), 76.5% (MAR), and 33.5% (Polar MM5) for the 1996 – 2008
611 period. The negative precipitation trends of $2.4 \pm 1.5 \% a^{-1}$ (Figure 10d) indicate a total of 2539.4 fewer Gt
612 of precipitation and a total of 5159.1 additional Gt of melt (not shown) over 1996 – 2013 across the GrIS.
613 Thus, our analysis suggests that a significant decline in snow accumulation contributes to declining SMB
614 throughout the Western GrIS over recent decades, in addition to increasing surface melt from rising
615 temperatures (van den Broeke et al., 2009, 2016).

616



617



618 **Figure 10.** Best fit linear trends for each grid cell showing magnitude (left) and percent (right) changes in total precipitation for a) and
 619 b) MAR (1996 – 2015) and c) and d) RACMO2 (1996 – 2013). Statistically significant RCM grid cell trends are stippled black. Also
 620 shown are accumulation trends for GreenTrACS firn cores (squares), ACT10A, ACT10B, ACT10C, D4, D5, Katie, Sandy, Summit 2010,
 621 and Raven/Dye-2 cores (stars on ice sheet) and precipitation trends from Mernild et al (2014; stars on coast) with statistically significant
 622 trends indicated by black dots.

623

624 **3.5. Effects of melt on accumulation trends**

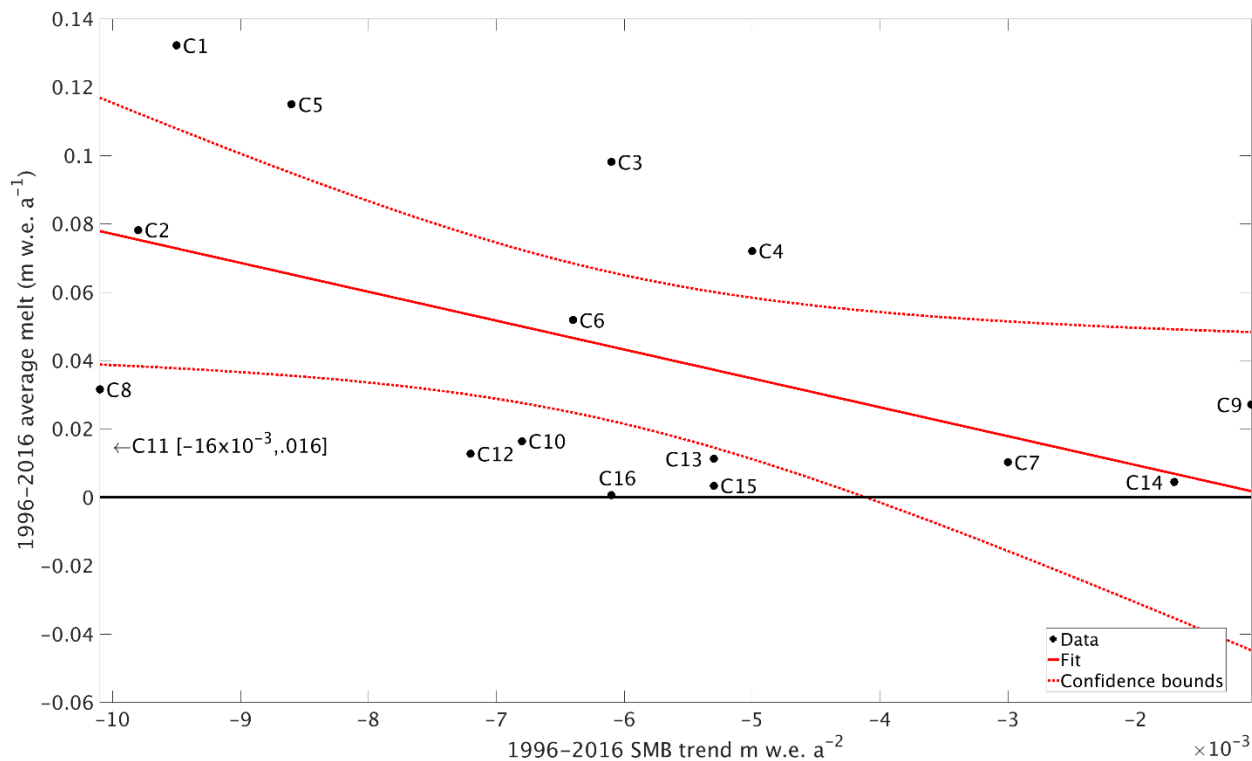
625 Increased melt throughout the 1996 – 2016 period is a confounding variable when analyzing trends in
 626 accumulation. With increased melt over the past several decades in this region, meltwater percolates down
 627 through several years of firn (Benson, 1962; Graeter et al., 2018; Harper et al., 2012; Wong et al., 2013).

628 This movement of mass into lower years can artificially increase the mass balance at depth and lower the
629 mass balance during the most recent years, which have not experienced as much meltwater percolation from
630 more recent annual layers. Therefore, it is necessary to evaluate the degree to which the recent accumulation
631 decrease in the GreenTrACS record is biased by the recent increase in surface melt and percolation.

632
633 Figure 11 compares the 1996 – 2016 mass balance trends with 1996 – 2016 average melt for each of the
634 sixteen GreenTrACS firn cores. If we exclude Core 11 (which only dates back to 1997 and has a highly
635 negative SMB trend), the linear regression is statistically significant with $p = 0.04$ (Figure 11). Note that both
636 the measured Core 11 SMB trend and RCM trends at that location are so negative, with that small amount of
637 average melt, that the linear trend is no longer significant if that point is included in the calculations. On
638 average, we find larger negative accumulation trends (-7×10^{-3} to -10×10^{-3} m w.e. a^{-2}) at the lower latitude
639 cores that experience more melt, supporting the hypothesis that meltwater percolation and refreezing are
640 enhancing the negative accumulation trend.

641
642 However, several other lines of evidence support a negative accumulation trend in the study area since 1996.
643 First, we find statistically significant negative accumulation trends at Cores 10, 11, 12, 13, 15, and 16, each
644 of which experience $< 1.6 \text{ cm } a^{-1}$ of meltwater percolation on average (Figure 11). Additionally, we have
645 confidence that GreenTrACS accumulation trends reported here are not artifacts of meltwater percolation
646 because both MAR and RACMO2 have similar trends in precipitation (Figure 10). Finally, we evaluate the
647 maximum effect meltwater percolation could have on GreenTrACS accumulation trends over 1996 – 2016.
648 The largest [measured](#) melt layer from our sixteen ice cores occurred during 2003 – 2004 in Core 1 and
649 contains 0.364 m of ice, equivalent to 0.333 m w.e. (Graeter et al., 2018). We add this percolation to nine
650 years' of accumulation using a sine wave (percolation magnitude 0, 0.5, 1, 0.5, 0, -0.5, -1, -0.5, 0), square
651 wave (0, 0, 0, 1, 1, 1, 0, 0, 0), and triangle wave (0, 0.25, 0.5, 0.75, 1, 0.75, 0.5, 0.25, 0) weighted kernel,
652 before re-computing hypothetical accumulation trends over the same time period with additional meltwater
653 percolation. Regardless of the wave-type choice, re-calculated trends remain within a factor of two of the
654 original SMB trends and do not change sign with additional percolation.

655



656

657 **Figure 11. Relationship between 1996 – 2016 SMB trend and 1996 – 2016 melt for each of the 16 GreenTrACS firn cores (black circles).**
 658 **Red line shows linear best fit, dotted line shows 95% confidence boundary.**

659

3.6. Atmospheric circulation drivers of the recent accumulation decline

660 Our analysis indicates that snow accumulation has been declining in Western Greenland since 1996, despite
 661 significant warming and resulting increases in saturation vapor pressure from the Clausius-Clapeyron
 662 relationship. Instead, precipitation decreases over Western Greenland likely result from changes in
 663 atmospheric and/or oceanic circulation. Mernild et al. (2014) and Auger et al. (2017) found that the positive
 664 phase of the Atlantic Multidecadal Oscillation (AMO) is associated with a precipitation increase over interior
 665 and Southwestern Greenland based on ice core records and the Japanese Meteorological Agency 55 Year
 666 Reanalysis (JRA-55; Kobayashi et al., 2015), respectively. In direct contrast with these findings, the decline
 667 in Western Greenland accumulation documented in the GreenTrACS record began in the mid-1990s,
 668 contemporaneous with a switch to the AMO positive phase.

669

670 We hypothesize that the differences between our results and those of Auger et al. (2017) and Mernild et al.
 671 (2014) stem from different causes. Auger et al. (2017) validated the reanalysis data by demonstrating that
 672 JRA-55 precipitation at Nuuk, Greenland is significantly correlated with Nuuk station data from 1958 – 2013.
 673 Furthermore, coastal precipitation in Western Greenland is strongly and significantly ($p < 0.05$) correlated
 674 with precipitation over the interior Western GrIS in the JRA-55 dataset (not shown). However, Mernild et al.
 675 (2014) found that coastal Greenland precipitation is anti-correlated with ice core accumulation records from

676 the interior GrIS from 1900 to 2000. This suggests that JRA-55 precipitation data, which is not constrained
677 by ice core accumulation records, should be interpreted with caution over the interior GrIS. Mernild et al.
678 (2014) concluded that positive AMO conditions favor higher precipitation over the interior GrIS based on
679 the previous positive AMO phase (1920s to mid-1960s), contrasting with lower accumulation during the
680 negative AMO phases (mid-1960s to mid-1990s and prior to the 1920s). However, Mernild et al. (2014) state
681 that the ice core composite record in their analysis may be biased from 1995 – 2000, and they do not analyze
682 precipitation trends after 2000. Thus, the decline in Western GrIS accumulation documented in the
683 GreenTrACS cores during the latest positive AMO phase from 1996 to 2017 was not captured in the Mernild
684 et al. (2014) analysis. Our results suggest that factors other than the AMO are behind the decline in Western
685 GrIS accumulation since 1996.

686
687 We find that the decrease in accumulation over the Western GrIS is associated with a significant decrease in
688 the number of storm-days since 1996. The GreenTrACS region experienced an average of 115.8 ± 15.3 storm-
689 days per year over 1958 – 1996 and 96.2 ± 27.3 storm-days per year over 1996 – 2016. A two sample t-test
690 indicates that this 17% decline in storm-days is statistically significant ($p < 0.001$). The largest decrease in
691 storm-days (25%) over the GreenTrACS region occurred during summer, with 56.4 ± 6.1 storm-days per
692 summer from 1958 – 1996 and 42.3 ± 17.4 storm-days per summer from 1996 – 2016 ($p < 0.0001$; Figure
693 12b). We also find an increase in the number of storm-days in the Northwestern GrIS near Thule (not shown).

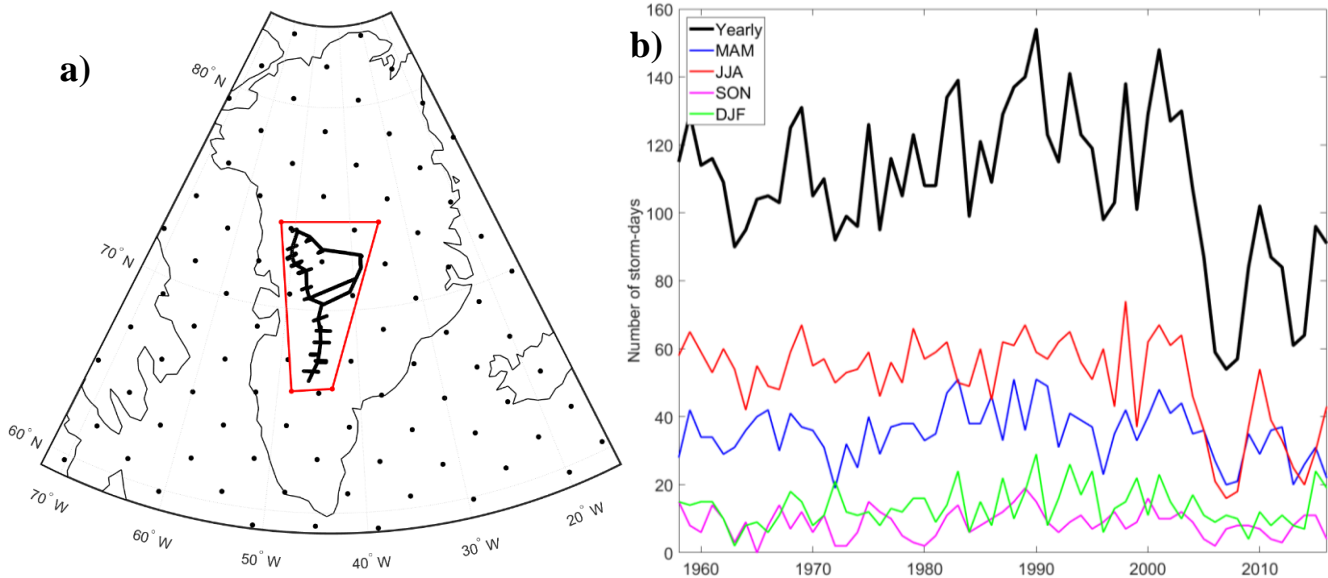
694
695 The decline in summer storm-days indicates a relationship with well-documented stronger summer blocking
696 over Greenland over the past two decades (Hanna et al., 2013; McLeod and Mote, 2016), with a positive
697 Greenland Blocking Index ([GBI](#)) during 17 out of 21 summers between 1996 – 2016 (Hanna et al., 2016).
698 The June – August GBI had a statistically significant positive trend of 1.87 (unitless; normalized to 1951 –
699 2000) from 1991 – 2015 (Hanna et al., 2016). The summertime 500 mbar geopotential height increased 50 –
700 70 m over the 1996 – 2016 period compared with the 1979 – 1996 baseline (Figure 12c), indicating stronger
701 blocking that we suggest likely reduced precipitation over the central GrIS by deflecting storms poleward
702 from the Greenland interior. This is consistent with an observed $0.9 \pm 0.3\%$ a^{-1} decrease in JJA cloud cover
703 over Greenland from 1995-2009, with the largest decreases in the GreenTrACS region (Hofer et al., 2017).
704 Furthermore, we find a strong negative correlation between ERA-Interim 1979 – 2015 June – August (JJA)
705 GBI and JJA precipitation in both MAR (Figure 12d) and RACMO2 (not shown) across the central and
706 southern GrIS. These results suggest that the blocking-induced accumulation decline observed in the
707 GreenTrACS region is representative of a broader pattern over the GrIS, with the exception of Northwest
708 Greenland where poleward blocking has increased storm-days (not shown) and accumulation (Figure 12d).

709

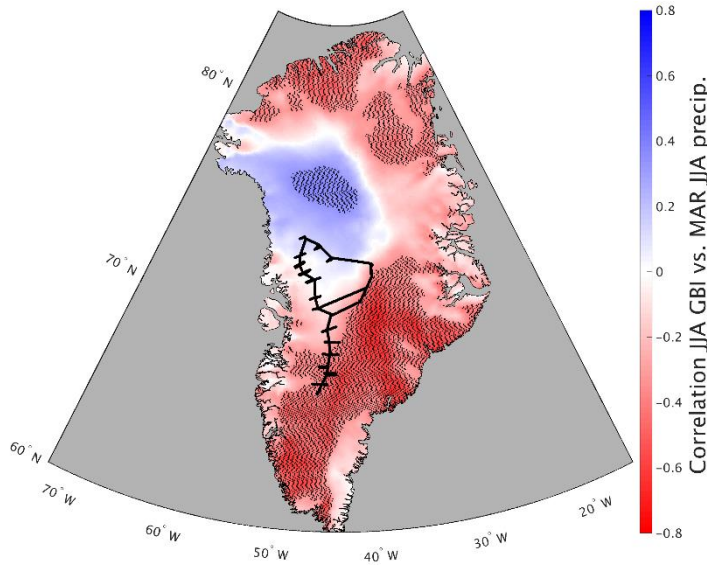
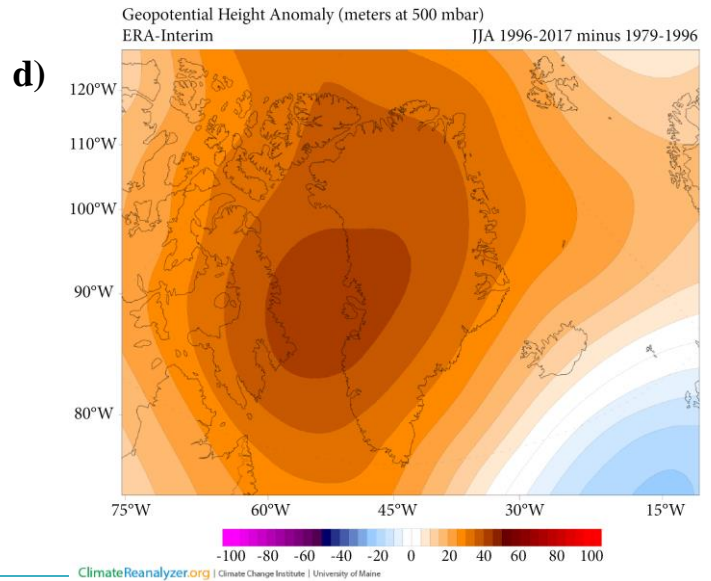
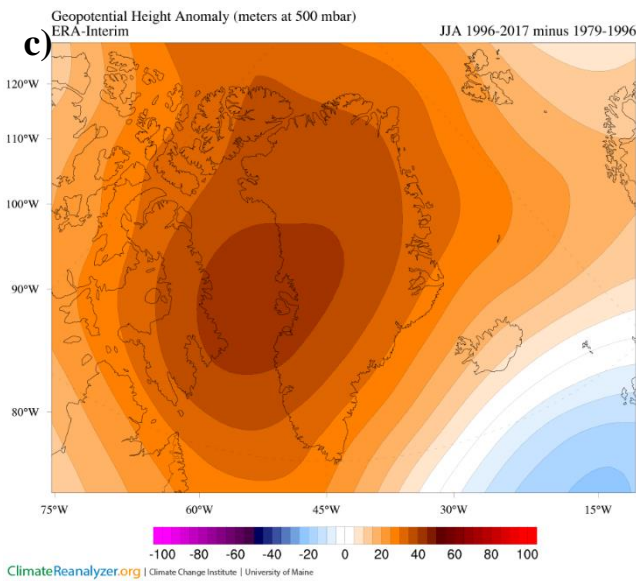
710

711 The effect of summertime Greenland blocking has [previously](#) been discussed primarily in the context of
712 increasing surface melt (Hanna et al., 2013; Ballinger et al., 2017; Hanna et al., 2018; Hofer et al., 2017),
713 while the effect of blocking on precipitation has received less attention (Hanna et al., 2013; McLeod and
714 Mote, 2016). Our results highlight that stronger summer blocking reduces GrIS SMB through both an
715 increase in surface melting and a decrease in accumulation. Stronger summer blocking has been tied to an
716 observed increase in surface melt since 1996 across the Western GrIS percolation zone (Graeter et al., 2018),
717 and to the July 2012 melt event, during which 98.6% of the GrIS experienced melt (Nghiem et al., 2012). We
718 show here with *in situ* data that snow accumulation has declined in this same region as strong blocking has
719 decreased the number of summer storm-days. Presently, none of the GBI outputs from the Coupled Model
720 Intercomparison Project 5 (CMIP5) suite of global climate models accurately capture the recent summer GBI
721 increase (Hanna et al., 2018). Improved predictions of summertime Greenland blocking under future
722 anthropogenic forcing scenarios are therefore critical for accurately predicting Greenland SMB and its
723 contribution to sea level rise.

724



725



726
727
728
729 **Figure 12. a)** (Serreze, 2009) gridded storm track dataset showing location of GreenTrACS traverse and inquiry box. **b)** Total number
730 of storm-days within inquiry box for annual and seasonal periods. Horizontal black lines show a decrease in 1958 – 1996 to 1996 – 2016
731 average number of storm-days within this region. **c)** 500 mbar geopotential height change over Greenland showing 1996 – 2016 minus
732 1979 – 1996 for the summer season. Image obtained using Climate Reanalyzer (<http://cci-reanalyzer.org>), Climate Change Institute,
733 University of Maine, United States. **d)** Correlation between June – August Greenland Blocking Index and MAR June – August
734 precipitation. Statistically significant RCM grid cell correlations are stippled black. GreenTrACS traverse is shown in black.

735 4. Conclusions

736 We have developed a new dataset of accumulation rates over the western interior of the Greenland ice sheet
737 spanning the past 20 – 60 years, based on sixteen 22 – 32 m long firn cores and 4436 km of *in situ* GPR
738 accumulation data. This accumulation record is internally consistent across the dataset and is validated by
739 previous *in situ* field measurements and other radar-derived accumulation measurements (e.g Lewis et al.,
740 2017).

741

742 Overall, the Polar MM5, ~~MAR, Box13, and RACMO2 Regional Climate Models accurately capture large~~
743 ~~spatial patterns in accumulation over the GrIS, but show statistically significant differences from GPR~~
744 ~~accumulation on a regional basis.~~ (Burgess et al., 2010), MAR (Fettweis et al., 2016), Box13 (Box et al.,
745 2013), and RACMO2 (Noël et al., 2018) Regional Climate Models accurately capture large spatial patterns
746 in accumulation over the GrIS, but show statistically significant differences from GPR accumulation on a
747 regional basis. The average RMS difference between each model and GreenTrACS accumulation is $0.068 \pm$
748 0.065 (MAR), 0.048 ± 0.045 (Polar MM5), 0.0822 ± 0.0702 (Box13), 0.0562 ± 0.0548 (RACMO2), and
749 0.0475 ± 0.0445 m w.e. a^{-1} (Bales09). These differences are on the same order as the uncertainties in the
750 GreenTrACS and RCM accumulation estimates. While these average differences are small, we find
751 differences of 0.1 to 0.4 m w.e. a^{-1} when we investigate at a local scale for each model.

752

753 While global climate models predict a 21st-century increase in precipitation over the GrIS (e.g. Bintanja and
754 Selten, 2014), we observe a decrease in precipitation across the Western GrIS from 1996 – 2016 using records
755 from firn cores, GPR, and published RCMs. We believe this study is the first to identify widespread negative
756 GrIS precipitation trends during this period of enhanced surface melt, evident in these RCMs and our field
757 observations (Graeter et al., 2018).

758

759 We attribute the decrease in accumulation over the Western GrIS between 1996 and 2016 to more persistently
760 positive Greenland blocking in the summer. We find a statistically significant 25% reduction in the number
761 of summer storms that precipitate over the GreenTrACS region since 1996. While warming temperatures
762 from anthropogenic forcing and enhanced summer blocking have increased melt across the western
763 percolation zone, here we show that summer blocking has also contributed to declining precipitation over the
764 past two decades. This has led to a strongly negative SMB trend on both the input and output sides of the
765 SMB equation that may not be accurately captured in global climate models that are currently unable to
766 reproduce the recent increase in blocking. This highlights the importance of improving GCM projections of
767 future summer blocking to accurately forecast Greenland precipitation and melt rates under stronger
768 greenhouse gas forcing.

769 5. Works cited

770 Auger, J. D., Birkel, S. D., Maasch, K. A., Mayewski, P. A. and Schuenemann, K. C.: Examination of
771 precipitation variability in southern Greenland, *J. Geophys. Res.*, 122(12), 6202–6216,
772 doi:10.1002/2016JD026377, 2017.

773 Bales, R. C., Guo, Q., Shen, D., McConnell, J. R., Du, G., Burkhart, J. F., Spikes, V. B., Hanna, E. and

774 Cappelen, J.: Annual accumulation for Greenland updated using ice core data developed during 2000-2006
775 and analysis of daily coastal meteorological data, *J. Geophys. Res. Atmos.*, 114(6), D06116,
776 doi:10.1029/2008JD011208, 2009.

777 Ballinger, T. J., Hanna, E., Hall, R. J., Cropper, T. E., Miller, J., Ribergaard, M. H., Overland, J. E. and
778 Høyer, J. L.: Anomalous blocking over Greenland preceded the 2013 extreme early melt of local sea ice,
779 *Ann. Glaciol.*, 2013(March 2013), 1–10, doi:10.1017/aog.2017.30, 2017.

780 Benson, C. S.: Stratigraphic studies in the snow and firn of the Greenland Ice Sheet, *Folia Geogr. Danica*, 9,
781 13–37, 1962.

782 Bevington, P. R. and Robinson, D. K.: *Data Reduction and Error Analysis for the Physical Sciences*, 2nd
783 Editio., McGraw-Hill., 1992.

784 Bintanja, R. and Selten, F. M.: Future increases in Arctic precipitation linked to local evaporation and sea-
785 ice retreat, *Nature*, 509(7501), 479–482, doi:10.1038/nature13259, 2014.

786 Box, J. E., Bromwich, D. H., Veenhuis, B. a., Bai, L. S., Stroeve, J. C., Rogers, J. C., Steffen, K., Haran, T.
787 and Wang, S. H.: Greenland Ice Sheet Surface Mass Balance Variability (1988 – 2004) from Calibrated
788 Polar MM5 Output *, *J. Clim.*, 19(12), 2783–2801, doi:doi.org/10.1175/JCLI3738.1, 2006.

789 Box, J. E., Cressie, N., Bromwich, D. H., Jung, J. H., van den Broeke, M. R., van Angelen, J. H., Forster, R.
790 R., Miège, C., Mosley-Thompson, E., Vinther, B. and McConnell, J. R.: Greenland ice sheet mass balance
791 reconstruction. Part I: Net snow accumulation (1600-2009), *J. Clim.*, 26(11), 3919–3934, doi:10.1175/JCLI-
792 D-12-00373.1, 2013.

793 van den Broeke, M. R., Bamber, J. L., Ettema, J., Rignot, E. J., Schrama, E., van de Berg, W. J., van
794 Meijgaard, E., Velicogna, I. and Wouters, B.: Partitioning recent Greenland mass loss., *Science*, 326(5955),
795 984–6, doi:10.1126/science.1178176, 2009.

796 van den Broeke, M. R., Enderlin, E. M., Howat, I. M., Kuipers Munneke, P., Noël, B., van de Berg, W. J.,
797 van Meijgaard, E. and Wouters, B.: On the recent contribution of the Greenland ice sheet to sea level change,
798 *Cryosph. Discuss.*, 1–26, doi:10.5194/tc-2016-123, 2016.

799 Brown, J., Harper, J., Pfeffer, W. T., Humphrey, N. and Bradford, J.: High-resolution study of layering within
800 the percolation and soaked facies of the Greenland ice sheet, *Ann. Glaciol.*, 52(59), 35–42,
801 doi:10.3189/172756411799096286, 2011.

802 Brown, J., Bradford, J., Harper, J., Pfeffer, W. T., Humphrey, N. and Mosley-Thompson, E.: Georadar-
803 derived estimates of firn density in the percolation zone, western Greenland ice sheet, *J. Geophys. Res. Earth
804 Surf.*, 117(1), 1–14, doi:10.1029/2011JF002089, 2012.

805 Buchardt, S. L., Clausen, H. B., Vinther, B. M. and Dahl-Jensen, D.: Investigating the past and recent $\delta^{18}O$ -
806 accumulation relationship seen in Greenland ice cores, *Clim. Past*, 8(6), 2053–2059, doi:10.5194/cp-8-2053-
807 2012, 2012.

808 Burgess, E. W., Forster, R. R., Box, J. E., Mosley-Thompson, E., Bromwich, D. H., Bales, R. C. and Smith,
809 L. C.: A spatially calibrated model of annual accumulation rate on the Greenland Ice Sheet (1958-2007), *J.
810 Geophys. Res. Earth Surf.*, 115(2), 1–14, doi:10.1029/2009JF001293, 2010.

811 Enderlin, E. M., Howat, I. M., Jeong, S., Noh, M. J., Van Angelen, J. H. and Van Den Broeke, M. R.: An
812 improved mass budget for the Greenland ice sheet, *Geophys. Res. Lett.*, 41(3), 866–872,
813 doi:10.1002/2013GL059010, 2014.

814 Fettweis, X., Box, J. E., Agosta, C., Amory, C., Kittel, C. and Gallée, H.: Reconstructions of the 1900-2015
815 Greenland ice sheet surface mass balance using the regional climate MAR model, *Cryosph. Discuss.*,
816 (November), 1–32, doi:10.5194/tc-2016-268, 2016.

817 Gerlitz, K., Knoll, M., Cross, G., Luzitano, R. and Knight, R.: Processing Ground Penetrating Radar Data to
818 Improve Resolution of Near-Surface Targets, in Symposium on the Application of Geophysics to
819 Engineering and Environmental Problems 1993, pp. 561–574, Environment and Engineering Geophysical
820 Society., 1993.

821 Graeter, K. A., Osterberg, E. C., Ferris, D., Hawley, R. L., Marshall, H. P. and Lewis, G.: Ice Core Records
822 of West Greenland Surface Melt and Climate Forcing, *Geophys. Res. Lett.*, doi:10.1002/2017GL076641,
823 2018.

824 Hall, D. K., Comiso, J. C., DiGirolamo, N. E., Shuman, C. A., Key, J. R. and Koenig, L. S.: A satellite-
825 derived climate-quality data record of the clear-sky surface temperature of the Greenland ice sheet, *J. Clim.*,
826 25(14), 4785–4798, 2012.

827 Hall, D. K., Comiso, J. C., DiGirolamo, N. E., Shuman, C. A., Box, J. E. and Koenig, L. S.: Variability in
828 the surface temperature and melt extent of the Greenland ice sheet from MODIS, *Geophys. Res. Lett.*, 40(10),
829 2114–2120, doi:10.1002/grl.50240, 2013.

830 Hanna, E., Mernild, S. H., Cappelen, J. and Steffen, K.: Recent warming in Greenland in a long-term
831 instrumental (1881–2012) climatic context: I. Evaluation of surface air temperature records, *Environ. Res.*
832 *Lett.*, 7(4), 045404, doi:10.1088/1748-9326/7/4/045404, 2012.

833 Hanna, E., Jones, J. M., Cappelen, J., Mernild, S. H., Wood, L., Steffen, K. and Huybrechts, P.: The influence
834 of North Atlantic atmospheric and oceanic forcing effects on 1900-2010 Greenland summer climate and ice
835 melt/runoff, *Int. J. Climatol.*, 33(4), 862–880, doi:10.1002/joc.3475, 2013.

836 Hanna, E., Cropper, T. E., Hall, R. J. and Cappelen, J.: Greenland Blocking Index 1851-2015: a regional
837 climate change signal, *Int. J. Climatol.*, 36(15), 4847–4861, doi:10.1002/joc.4673, 2016.

838 Hanna, E., Fettweis, X. and Hall, R. J.: Recent changes in summer Greenland blocking captured by none of
839 the CMIP5 models, *Cryosph. Discuss.*, 1–8, doi:10.5194/tc-2018-91, 2018.

840 Harper, J., Humphrey, N., Pfeffer, W. T., Brown, J. and Fettweis, X.: Greenland ice-sheet contribution to
841 sea-level rise buffered by meltwater storage in firn, *Nature*, 491(7423), 240–243, doi:10.1038/nature11566,
842 2012.

843 Hawley, R. L., Courville, Z. R., Kehrl, L. M., Lutz, E. R., Osterberg, E. C., Overly, T. B. and Wong, G. J.:
844 Recent accumulation variability in northwest Greenland from ground-penetrating radar and shallow cores
845 along the Greenland Inland Traverse, *J. Glaciol.*, 60(220), 375–382, doi:10.3189/2014JoG13J141, 2014.

846 Herron, M. M. and Langway, C. C.: Firn densification: an empirical model., *J. Glaciol.*, 25(93), 373–385,
847 doi:10.3198/1980JoG25-93-373-385, 1980.

848 Hofer, S., Bamber, J., Tedstone, A. and Fettweis, X.: Decreasing clouds drive mass loss on the Greenland
849 Ice Sheet, *EGU Gen. Assem. Conf. Abstr.*, 19(6), 5086, 2017.

850 Karlöf, L., Isaksson, E., Winther, J. G., Gundestrup, N. S., Meijer, H. A. J., Mulvaney, R., Pourchet, M.,
851 Hofstede, C., Lappégard, G., Petterson, R., van den Broeke, M. R. and Van De Wal, R. S. W.: Accumulation
852 variability over a small area in east Dronning Maud Land, Antarctic, as determined from shallow firn cores
853 and snow pits: Some implications for ice-core records, *J. Glaciol.*, 51(174), 343–352,
854 doi:10.3189/172756505781829232, 2005.

855 Kobayashi, S., Ota, Y., Harada, Y., Ebata, A., Moriya, M., Onoda, H., Onogi, K., Kamahori, H., Kobayashi,
856 C., Endo, H., Miyaoka, K. and Takahashi, K.: The JRA-55 Reanalysis: General Specifications and Basic
857 Characteristics, *J. Meteorol. Soc. Japan. Ser. II*, 93(1), 5–48, doi:10.2151/jmsj.2015-001, 2015.

858 Koenig, L. S., Ivanoff, A., Alexander, P. M., MacGregor, J. A., Fettweis, X., Panzer, B., Paden, J. D., Forster,
859 R. R., Das, I., McConnell, J. R., Tedesco, M., Leuschen, C. and Gogineni, S. P.: Annual Greenland
860 accumulation rates (2009–2012) from airborne snow radar, *Cryosph.*, 10(4), 1739–1752, doi:10.5194/tc-10-

861 1739-2016, 2016.

862 Kovacs, A., Gow, A. J. and Morey, R. M.: The in-situ dielectric constant of polar firn revisited, *Cold Reg. Sci. Technol.*, 23(3), 245–256, doi:10.1016/0165-232X(94)00016-Q, 1995.

864 De La Peña, S., Howat, I. M., Nienow, P. W., Van Den Broeke, M. R., Mosley-Thompson, E., Price, S. F., Mair, D., Noël, B. and Sole, A. J.: Changes in the firn structure of the western Greenland Ice Sheet caused by recent warming, *Cryosphere*, 9(3), 1203–1211, doi:10.5194/tc-9-1203-2015, 2015.

867 Lavielle, M.: Using penalized contrasts for the change-point problem, *Signal Processing*, 85(8), 1501–1510, doi:10.1016/j.sigpro.2005.01.012, 2005.

869 Lewis, G., Osterberg, E. C., Hawley, R. L., Whitmore, B., Marshall, H. P. and Box, J. E.: Regional Greenland accumulation variability from Operation IceBridge airborne accumulation radar, *Cryosph.*, 11(2), 773–788, doi:10.5194/tc-11-773-2017, 2017.

872 McLeod, J. T. and Mote, T. L.: Linking interannual variability in extreme Greenland blocking episodes to the recent increase in summer melting across the Greenland ice sheet, *Int. J. Climatol.*, 36(3), 1484–1499, doi:10.1002/joc.4440, 2016.

875 Medley, B., Joughin, I., Das, S. B., Steig, E. J., Conway, H., Gogineni, S. P., Criscitiello, a. S., McConnell, J. R., Smith, B. E., van den Broeke, M. R., Lenaerts, J. T. M., Bromwich, D. H. and Nicolas, J. P.: Airborne-radar and ice-core observations of annual snow accumulation over Thwaites Glacier, West Antarctica confirm the spatiotemporal variability of global and regional atmospheric models, *Geophys. Res. Lett.*, 40(14), 3649–3654, doi:10.1002/grl.50706, 2013.

880 Mernild, S. H., Hanna, E., McConnell, J. R., Sigl, M., Beckerman, A. P., Yde, J. C., Cappelen, J., Malmros, J. K. and Steffen, K.: Greenland precipitation trends in a long-term instrumental climate context (1890-2012): Evaluation of coastal and ice core records, *Int. J. Climatol.*, doi:10.1002/joc.3986, 2014.

883 Meyer, C. R. and Hewitt, I. J.: A continuum model for meltwater flow through compacting snow, *Cryosphere*, 11(6), 2799–2813, doi:10.5194/tc-11-2799-2017, 2017.

885 Morlighem, M., Rignot, E. J., Mouginot, J., Seroussi, H. and Larour, E.: Deeply incised submarine glacial valleys beneath the Greenland ice sheet, *Nat. Geosci.*, 7(6), 18–22, doi:10.1038/ngeo2167, 2014.

887 Morris, E. M. and Wingham, D. J.: Densification of polar snow: Measurements, modeling, and implications for altimetry, *J. Geophys. Res. Earth Surf.*, 119(2), 349–365, doi:10.1002/2013JF002898, 2014.

889 Mosley-Thompson, E., McConnell, J. R., Bales, R. C., Li, Z., Lin, P.-N., Steffen, K., Thompson, L. G., Edwards, R. and Bathke, D.: Local to regional-scale variability of annual net accumulation on the Greenland ice sheet from PARCA cores, *J. Geophys. Res.*, 106(D24), 33839, doi:10.1029/2001JD900067, 2001.

892 Mouginot, J., Rignot, E., Bjørk, A. A., van den Broeke, M., Millan, R., Morlighem, M., Noël, B., Scheuchl, B. and Wood, M.: Forty-six years of Greenland Ice Sheet mass balance from 1972 to 2018, *Proc. Natl. Acad. Sci.*, 201904242, doi:10.1073/pnas.1904242116, 2019.

895 Nghiem, S. V., Steffen, K., Neumann, G. and Huf, R.: Mapping of ice layer extent and snow accumulation in the percolation zone of the Greenland ice sheet, *J. Geophys. Res. Earth Surf.*, 110(2), 1–13, doi:10.1029/2004JF000234, 2005.

898 Nghiem, S. V., Hall, D. K., Mote, T. L., Tedesco, M., Albert, M. R., Keegan, K. M., Shuman, C. A., DiGirolamo, N. E. and Neumann, G.: The extreme melt across the Greenland ice sheet in 2012, *Geophys. Res. Lett.*, 39(20), 6–11, doi:10.1029/2012GL053611, 2012.

901 Noël, B., van de Berg, W. J., Van Wessem, J. M., Van Meijgaard, E., Van As, Di., Lenaerts, J. T. M., Lhermitte, S., Munneke, P. K., Smeets, C. J. P. P., Van Ulf, L. H., Van De Wal, R. S. W. and Van Den Broeke, M. R.: Modelling the climate and surface mass balance of polar ice sheets using RACMO2 - Part 1:

- 904 Greenland (1958-2016), *Cryosphere*, 12(3), 811–831, doi:10.5194/tc-12-811-2018, 2018.
- 905 Nye, J. F.: Correction factor for accumulation measured by the thickness of the annual layers in an ice sheet,
906 *J. Glaciol.*, 4(36), 785–788, 1963.
- 907 Osterberg, E. C., Handley, M. J., Sneed, S. B., Mayewski, P. A. and Kreutz, K. J.: Continuous ice core melter
908 system with discrete sampling for major ion, trace element, and stable isotope analyses, *Environ. Sci.*
909 *Technol.*, 40(10), 3355–3361, doi:10.1021/es052536w, 2006.
- 910 Osterberg, E. C., Hawley, R. L., Wong, G. J., Kopec, B., Ferris, D. and Howley, J.: Coastal ice-core record
911 of recent northwest Greenland temperature and sea-ice concentration, *J. Glaciol.*, 61(230), 1137–1146,
912 doi:10.3189/2015JoG15J054, 2015.
- 913 Overly, T. B., Hawley, R. L., Helm, V., Morris, E. M. and Chaudhary, R. N.: Greenland annual accumulation
914 along the EGIG line, 1959–2004, from ASIRAS airborne radar and neutron-probe density measurements,
915 *Cryosph.*, 10(4), 1679–1694, doi:10.5194/tc-10-1679-2016, 2016.
- 916 Rennermalm, A. K., Moustafa, S. E., Mioduszewski, J., Chu, V. W., Forster, R. R., Hagedorn, B., Harper, J.
917 T., Mote, T. L., Robinson, D. A., Shuman, C. A., Smith, L. C. and Tedesco, M.: Understanding Greenland
918 ice sheet hydrology using an integrated multi-scale approach, *Environ. Res. Lett.*, 8(1), 015017,
919 doi:10.1088/1748-9326/8/1/015017, 2013.
- 920 Rodriguez-Morales, F., Gogineni, S. P., Leuschen, C. J., Paden, J. D., Li, J., Lewis, C. C., Panzer, B., Gomez-
921 Garcia Alvestegui, D., Patel, A., Byers, K., Crowe, R., Player, K., Hale, R. D., Arnold, E. J., Smith, L.,
922 Gifford, C. M., Braaten, D. and Panton, C.: Advanced multifrequency radar instrumentation for polar
923 Research, *IEEE Trans. Geosci. Remote Sens.*, 52(5), 2824–2842, doi:10.1109/TGRS.2013.2266415, 2014.
- 924 Sasgen, I., van den Broeke, M. R., Bamber, J. L., Rignot, E. J., Sorensen, L. S., Wouters, B., Martinec, Z.,
925 Velicogna, I. and Simonsen, S. B.: Timing and origin of recent regional ice-mass loss in Greenland, *Earth*
926 *Planet. Sci. Lett.*, 333–334, 293–303, doi:10.1016/j.epsl.2012.03.033, 2012.
- 927 Selesnick, I. W. and Sidney Burrus, C.: Generalized digital butterworth filter design, *IEEE Trans. Signal*
928 *Process.*, 46(6), 1688–1694, doi:10.1109/78.678493, 1998.
- 929 Serreze, M.: Northern Hemisphere cyclone locations and characteristics from NCEP/NCAR reanalysis data,
930 Verison 1, Natl. Snow Ice Data Center, Boulder, CO, Digit. media.[Available online <http://nsidc.org/data/nsidc-0423.html>], 2009.
- 931
- 932 Spikes, V. B., Hamilton, G. S., Arcone, S. A., Kaspari, S. and Mayewski, P. A.: Variability in accumulation
933 rates from GPR profiling on the West Antarctic plateau, *Ann. Glaciol.*, 39, 238–244,
934 doi:10.3189/172756404781814393, 2004.
- 935 Trusel, L. D., Das, S. B., Osman, M. B., Evans, M. J., Smith, B. E., Fettweis, X., McConnell, J. R., Noël, B.
936 and van den Broeke, M. R.: Nonlinear rise in Greenland runoff in response to post-industrial Arctic warming,
937 *Nature*, 564(7734), 104–108, doi:10.1038/s41586-018-0752-4, 2018.
- 938 Vandecrux, B., Fausto, R. S., Langen, P. L., Van As, D., MacFerrin, M., Colgan, W., Ingeman-Nielsen, T.,
939 Steffen, K., Jensen, N. S., Møller, M. T. and Box, J. E.: Drivers of Firn Density on the Greenland Ice Sheet
940 Revealed by Weather Station Observations and Modelling, *J. Geophys. Res. Earth Surf.*,
941 doi:10.1029/2017JF004597, 2018.
- 942 Vernon, C. L., Bamber, J. L., Box, J. E., Van Den Broeke, M. R., Fettweis, X., Hanna, E. and Huybrechts,
943 P.: Surface mass balance model intercomparison for the Greenland ice sheet, *Cryosph.*, 7(5), 599–614,
944 doi:10.5194/tc-7-599-2013, 2013.
- 945 Wong, G. J., Hawley, R. L., Lutz, E. R. and Osterberg, E. C.: Trace-element and physical response to melt
946 percolation in Summit (Greenland) snow, *Ann. Glaciol.*, 54(63), 52–62, doi:10.3189/2013aog63a602, 2013.

- 947 Wong, G. J., Osterberg, E. C., Hawley, R. L., Courville, Z. R., Ferris, D. G. and Howley, J.: Coast-to-interior
948 gradient in recent northwest Greenland precipitation trends (1952 – 2012), Environ. Res. Lett., 10(11),
949 114008, doi:10.1088/1748-9326/10/11/114008, 2015.
- 950 Yilmaz, Ö.: Seismic Data Analysis, Society of Exploration Geophysicists., 2001.
- 951 Zumberge, J. F., Heflin, M. B., Jefferson, D. C., Watkins, M. M. and Webb, F. H.: Precise point positioning
952 for the efficient and robust analysis of GPS data from large networks, J. Geophys. Res. Solid Earth, 102(B3),
953 5005–5017, doi:10.1029/96JB03860, 1997.
- 954